

CDPA: Common and Distinctive Pattern Analysis between High-dimensional Datasets

Zhe Qu^a, and Hai Shu^{b*}

^aDepartment of Mathematics, Tulane University, New Orleans, LA, 70118

^bDepartment of Biostatistics, New York University, New York, NY, 10012

Abstract

A representative model in integrative analysis of two high-dimensional data types is to decompose each data matrix into a low-rank common matrix generated by latent factors shared across data types, a low-rank distinctive matrix corresponding to each data type, and an additive noise matrix. Existing decomposition methods claim that their common matrices capture the common pattern of the two data types. However, their so-called common pattern only denotes the common latent factors but ignores the common information between the two coefficient matrices of these latent factors. We propose a novel method, called the common and distinctive pattern analysis, which appropriately defines the two patterns by further incorporating the common and distinctive information of the coefficient matrices. A consistent estimation approach is developed for high-dimensional settings, and shows reasonably good finite-sample performance in simulations. We illustrate the superiority of proposed method over the state-of-the-art by real-world data examples obtained from Human Connectome Project and The Cancer Genome Atlas.

Keywords: Canonical variable; Data integration; Graph matching; Mixing channel; Principal vector.

*Contact for correspondence: Hai Shu, Ph.D.; e-mail: hs120@nyu.edu.

1 Introduction

Modern biomedical studies often collect multiple types of large-scale datasets on a common set of objects (Crawford et al., 2016; Jensen et al., 2017). For example, The Cancer Genome Atlas (TCGA; Hoadley et al., 2018) collected for tumor samples the multi-platform genomic data such as mRNA expression and DNA methylation. The Human Connectome Project (HCP; Van Essen et al., 2013) also acquired from healthy adults the multi-modal brain images including structural MRI and functional MRI. The use of multiple data types can allow us to enhance understanding the mechanisms underlying complex diseases like cancers (Koboldt et al., 2012; Campbell et al., 2018) and neurodegenerative diseases (Weiner et al., 2013; Saeed et al., 2017), or to improve the performance in various learning tasks such as clustering (Lock et al., 2013) and classification (Zhou et al., 2016).

The most straightforward approach to the integrative analysis of multi-type datasets is to concatenate all their data matrices into one matrix and then implement standard data analysis tools. One such example is the simultaneous component analysis (SCA; Smilde et al., 2003), which applies the principal component analysis (PCA) to the concatenated data matrix and thus is also known as SUM-PCA. These methods are simple to implement, but they are unable to explore or interpret the relationships among datasets. As pioneers to overcome this drawback, the canonical correlation analysis (CCA; Hotelling, 1936) and its various generalizations (Carroll, 1968; Kettenring, 1971) measure the correlations and extract the most correlated components among datasets. The CCA methods only account for correlated features and fail to reveal a more detailed relationship on the common and distinctive patterns across datasets.

A family of data integration methods has emerged recently to identify and separate the common and distinctive variations across datasets, including orthogonal n -block partial least squares (OnPLS; Löfstedt and Trygg, 2011), distinctive and common components with SCA (DISCO-SCA; Schouteden et al., 2013), common orthogonal basis extraction (COBE; Zhou et al., 2016), joint and individual variation explained (JIVE; Lock et al., 2013) and its variants (O’Connell and Lock, 2016; Feng et al., 2018), and decomposition-based CCA (D-CCA; Shu et al., 2019). Consider the case with two datasets. All these methods decompose each data matrix into a low-rank “common” matrix generated by latent factors shared across datasets, a low-rank “distinctive” matrix corresponding to each dataset, and an additive noise matrix. Despite different constraints in

the decomposition, these methods refer the common pattern of the two datasets to the common latent factors, but ignore the common information between the two coefficient matrices of these latent factors. It may be more appropriate to name their “common” and “distinctive” matrices as “common-source” and “distinctive-source” matrices.

We propose a new method, called the common and distinctive pattern analysis (CDPA), to improve the delineation of the common and distinctive patterns between two datasets. The CDPA method defines the common pattern by incorporating both the common latent factors and the common information of their coefficient matrices, and determines each distinctive pattern as the residual part of the corresponding signal dataset. The coefficient matrices are called mixing channels in signal processing (Papadias, 2000; Parra and Sajda, 2003), which introduce correlations into the uncorrelated source variables to generate the output data. Hence, the common and distinctive information in the coefficient matrices is also important and should be separated into the common and distinctive patterns of the two datasets. Our defined common-pattern and distinctive-pattern matrices together with the aforementioned common-source and distinctive-source matrices constitute a more comprehensive picture that depicts the relationship of two datasets.

Three challenging issues arise in the construction and estimation of common-pattern and distinctive-pattern matrices: (i) There exists the row matching problem of the two coefficient matrices, or equivalently the variable pairing problem of the two datasets, if the rows of either observed data matrix can be arbitrarily ordered independent of the other matrix; (ii) The common information of the two coefficient matrices must be identified; (iii) Recovering the high-dimensional common-pattern and distinctive-pattern matrices confronts the curse of dimensionality where the unknown large covariance matrices may not be consistently estimated by the traditional sample covariance matrices (Yin et al., 1988). We successfully convert the row matching problem (i) into the classic graph matching problem (Lu et al., 2016). We extract the common information in (ii) by our extended analogy of the state-of-the-art D-CCA. To address the challenge (iii), we develop consistent estimators of proposed common-pattern and distinctive-pattern matrices under the high-dimensional spiked covariance model (Fan et al., 2013; Wang and Fan, 2017; Shu et al., 2019), which has been widely used in various fields, such as signal processing (Nadakuditi and Silverstein, 2010), machine learning (Huang, 2017), and economics (Chamber-

lain and Rothschild, 1983).

The rest of this article is organized as follows. Section 2 introduces the CCA and D-CCA methods as preliminaries. Our CDPA method and its consistent estimation are established in Section 3. The finite-sample performance of proposed estimators is investigated via simulations in Section 4. Section 5 compares the proposed CDPA method with the state-of-the-art D-CCA in two real-data examples, respectively, from HCP and TCGA. All theoretical proofs and additional simulation results are provided in the Supplementary Material.

2 Preliminaries

Let $\mathbf{Y}_k \in \mathbb{R}^{p_k \times n}$ for $k \in \{1, 2\}$ be the k -th mean-centered dataset obtained on a common set of n objects, where p_k is the number of variables. The decomposition model considered in aforementioned existing methods (e.g., D-CCA) is

$$\mathbf{Y}_k = \mathbf{X}_k + \mathbf{E}_k = \mathbf{C}_k + \mathbf{D}_k + \mathbf{E}_k \in \mathbb{R}^{p_k \times n} \quad (1)$$

for which the n columns of each matrix are assumed to be independent and identically distributed (i.i.d.) samples of the corresponding mean-zero random vector in

$$\mathbf{y}_k = \mathbf{x}_k + \mathbf{e}_k = \mathbf{c}_k + \mathbf{d}_k + \mathbf{e}_k \in \mathbb{R}^{p_k} \quad (2)$$

where $\{\mathbf{X}_k, \mathbf{x}_k\}_{k=1}^2$ and $\{\mathbf{E}_k, \mathbf{e}_k\}_{k=1}^2$ are signals and noises, respectively, $\{\mathbf{C}_k\}_{k=1}^2$ and $\{\mathbf{c}_k\}_{k=1}^2$ are common-source matrices and random vectors that are generated from the common latent factors of the two datasets, and \mathbf{D}_k and \mathbf{d}_k are the distinctive-source matrix and random vector from distinctive latent factors of the k -th dataset. Write each k -th common-source random vector by $\mathbf{c}_k = \mathbf{B}_k([c_\ell]_{\ell=1}^{L_{12}})^\top$, where $[c_\ell]_{\ell=1}^{L_{12}} = (c_1, \dots, c_{L_{12}})$ are the common latent factors and \mathbf{B}_k is the coefficient matrix of $[c_\ell]_{\ell=1}^{L_{12}}$ for \mathbf{c}_k . The common information of \mathbf{B}_1 and \mathbf{B}_2 is not considered by the existing methods, which motivates our current research.

We start with signal vectors $\{\mathbf{x}_k\}_{k=1}^2$ for simplicity, and introduce the CCA and D-CCA methods, respectively, in the two subsections of this section. The signal estimation is deferred to Section 3.3. We now introduce some notation. For a $p \times n$ real matrix $\mathbf{M} = (M_{ij})_{1 \leq i \leq p, 1 \leq j \leq n}$, denote the ℓ -th largest singular value and the ℓ -th largest eigenvalue (if $p = n$) by $\sigma_\ell(\mathbf{M})$

and $\lambda_\ell(\mathbf{M})$ respectively, the spectral norm $\|\mathbf{M}\|_2 = \sigma_1(\mathbf{M})$, the Frobenius norm $\|\mathbf{M}\|_F = \sqrt{\sum_{i=1}^p \sum_{j=1}^n M_{ij}^2}$, the matrix \mathcal{L}^∞ norm $\|\mathbf{M}\|_\infty = \max_{1 \leq i \leq p} \sum_{j=1}^n |M_{ij}|$, and the max norm $\|\mathbf{M}\|_{\max} = \max_{i,j} |M_{ij}|$. Let $\mathbf{M}^{[s:t,u:v]}$, $\mathbf{M}^{[s:t,:]}$ and $\mathbf{M}^{[:,u:v]}$ denote the submatrices $(M_{ij})_{s \leq i \leq t, u \leq j \leq v}$, $(M_{ij})_{s \leq i \leq t, 1 \leq j \leq n}$ and $(M_{ij})_{1 \leq i \leq p, u \leq j \leq v}$ of \mathbf{M} , respectively. Write the Moore-Penrose pseudoinverse of \mathbf{M} by \mathbf{M}^\dagger , and the column space of \mathbf{M} by $\text{colsp}(\mathbf{M})$. Denote the $p \times n$ zero matrix by $\mathbf{0}_{p \times n}$, and the $p \times p$ identity matrix by $\mathbf{I}_{p \times p}$. Define $\text{diag}(\mathbf{M}_1, \dots, \mathbf{M}_m)$ to be a block diagonal matrix with $\mathbf{M}_1, \dots, \mathbf{M}_m$ as its main diagonal blocks. Let $[\mathbf{M}_1; \mathbf{M}_2] = [\mathbf{M}_1^\top, \mathbf{M}_2^\top]^\top$ for matrices \mathbf{M}_1 and \mathbf{M}_2 with the same number of columns. Denote the j -th entry of a vector \mathbf{v} by $\mathbf{v}^{[j]}$. Write $\text{span}(\mathbf{v}^\top) = \text{span}(\{v_j\}_{j=1}^p) = \{\sum_{j=1}^p a_j v_j : \forall a_j \in \mathbb{R}\}$ for any vector $\mathbf{v} = (v_1, \dots, v_p)^\top$. For vectors $\{\mathbf{v}_\ell\}_{\ell=1}^L$, let $[\mathbf{v}_\ell]_{\ell=1}^L = (\mathbf{v}_1, \dots, \mathbf{v}_L)$. For a subspace B of a vector space A , denote its orthogonal complement in A by $A \setminus B$. Denote the angle between two elements v_1 and v_2 in their inner product space by $\theta(v_1, v_2)$. Let $(\mathcal{L}_0^2, \text{cov})$ be the inner product space composed of all real-valued random variables with zero mean and finite variance, and endowed with the covariance operator as the inner product. Note that in $(\mathcal{L}_0^2, \text{cov})$, $\cos \theta(\cdot, \cdot) = \text{corr}(\cdot, \cdot)$ and $\|\cdot\| = \sqrt{\text{var}(\cdot)}$. Write $a \propto b$ if a is proportional to b , namely, $a = \kappa b$ for some constant κ . Denote $a \vee b = \max(a, b)$ and $a \wedge b = \min(a, b)$. Let both $x := y$ and $y =: x$ mean that x is defined by y . Denote the equivalence between two statements S_1 and S_2 by $S_1 \Leftrightarrow S_2$. For signal vectors $\{\mathbf{x}_k\}_{k=1}^2$, denote $\Sigma_k = \text{cov}(\mathbf{x}_k)$, $\Sigma_{12} = \text{cov}(\mathbf{x}_1, \mathbf{x}_2)$, $r_k = \text{rank}(\Sigma_k)$, $r_{\min} = \min(r_1, r_2)$, $r_{\max} = \max(r_1, r_2)$, and $r_{12} = \text{rank}(\Sigma_{12})$. Throughout the paper, our asymptotic arguments are by default under $n \rightarrow \infty$.

2.1 Canonical correlation analysis

The CCA method (Hotelling, 1936) sequentially finds the most correlated variables, called canonical variables, between the two subspaces $\{\text{span}(\mathbf{x}_k^\top)\}_{k=1}^2$ in $(\mathcal{L}_0^2, \text{cov})$. For $1 \leq \ell \leq r_{12}$, the ℓ -th pair of canonical variables are defined by

$$\begin{aligned} \{z_{1\ell}, z_{2\ell}\} \in \arg \max_{\{z_k\}_{k=1}^2} \text{corr}(z_1, z_2) \quad \text{subject to} \\ \text{var}(z_k) = 1 \text{ and } z_k \in \text{span}(\mathbf{x}_k^\top) \setminus \text{span}(\{z_{km}\}_{m=1}^{\ell-1}), \end{aligned} \tag{3}$$

where $\text{span}(\mathbf{x}_k^\top) \setminus \text{span}(\{z_{km}\}_{m=1}^0) := \text{span}(\mathbf{x}_k^\top)$. The correlation $\rho_\ell := \text{corr}(z_{1\ell}, z_{2\ell})$ is called the ℓ -th canonical correlation of \mathbf{x}_1 and \mathbf{x}_2 . Augment $\{z_{k\ell}\}_{\ell=1}^{r_{12}}$ with any $(r_k - r_{12})$ standardized

variables to be $\mathbf{z}_k = (z_{k1}, \dots, z_{kr_k})^\top$ such that \mathbf{z}_k^\top is an orthonormal basis of $\text{span}(\mathbf{x}_k^\top)$. We have the bi-orthogonality (Shu et al., 2019) that

$$\text{cov}(\mathbf{z}_1, \mathbf{z}_2) = \text{diag}(\rho_1, \dots, \rho_{r_{12}}, \mathbf{0}_{(r_1-r_{12}) \times (r_2-r_{12})}). \quad (4)$$

The augmented canonical variables $\{\mathbf{z}_1, \mathbf{z}_2\}$ can be obtained by

$$\mathbf{z}_k = \mathbf{U}_{\theta_k}^\top \mathbf{z}_k^*, \quad (5)$$

where $\mathbf{z}_k^* = \mathbf{\Lambda}_k^{-1/2} \mathbf{V}_k^\top \mathbf{x}_k$, $\mathbf{\Sigma}_k = \mathbf{V}_k \mathbf{\Lambda}_k \mathbf{V}_k^\top$ is a compact singular value decomposition (SVD) with $\mathbf{\Lambda}_k = \text{diag}(\sigma_1(\mathbf{\Sigma}_k), \dots, \sigma_{r_k}(\mathbf{\Sigma}_k))$, and $\mathbf{\Theta} := \text{cov}(\mathbf{z}_1^*, \mathbf{z}_2^*) = \mathbf{U}_{\theta_1} \mathbf{\Lambda}_\theta \mathbf{U}_{\theta_2}^\top$ is a full SVD with $\mathbf{\Lambda}_\theta = \text{diag}(\rho_1, \dots, \rho_{r_{12}}, \mathbf{0}_{(r_1-r_{12}) \times (r_2-r_{12})})$.

A similar method to CCA is the principal angle analysis (PAA; Björck and Golub, 1973), which investigates the closeness of any two subspaces, denoted by F and G , in the Euclidean dot product space (\mathbb{R}^n, \cdot) . For $1 \leq \ell \leq q := \min\{\dim(F), \dim(G)\}$, the ℓ -th principal angle $\theta_\ell \in [0, \pi/2]$ between F and G is defined by

$$\begin{aligned} \cos \theta_\ell &= \max_{\mathbf{u} \in F} \max_{\mathbf{v} \in G} \mathbf{u}^\top \mathbf{v} = \mathbf{u}_\ell^\top \mathbf{v}_\ell \quad \text{subject to} \\ \|\mathbf{u}\|_F &= \|\mathbf{v}\|_F = 1, \text{ and } \mathbf{u}^\top \mathbf{u}_j = \mathbf{v}^\top \mathbf{v}_j = 0 \text{ for } j = 1, \dots, \ell - 1. \end{aligned} \quad (6)$$

The vectors $\{\mathbf{u}_\ell, \mathbf{v}_\ell\}$ are called the ℓ -th pair of principal vectors of F and G . Let \mathbf{Q}_F and \mathbf{Q}_G be the matrices whose columns form the orthonormal bases of F and G , respectively. The principal angles and principal vectors can be obtained by

$$\cos \theta_\ell = \sigma_\ell(\mathbf{Q}_F^\top \mathbf{Q}_G), \quad (\mathbf{u}_1, \dots, \mathbf{u}_q) = \mathbf{Q}_F \mathbf{U}_Q, \quad (\mathbf{v}_1, \dots, \mathbf{v}_q) = \mathbf{Q}_G \mathbf{V}_Q, \quad (7)$$

where $\mathbf{Q}_F^\top \mathbf{Q}_G = \mathbf{U}_Q \text{diag}\{\sigma_1(\mathbf{Q}_F^\top \mathbf{Q}_G), \dots, \sigma_q(\mathbf{Q}_F^\top \mathbf{Q}_G)\} \mathbf{V}_Q^\top$ is a SVD of $\mathbf{Q}_F^\top \mathbf{Q}_G$.

The PAA and CCA methods are essentially the same except their respective inner product spaces (\mathbb{R}^n, \cdot) and $(\mathcal{L}_0^2, \text{cov})$. The principal vectors and the cosines of principal angles of PAA correspond to the canonical variables and the canonical correlations of CCA. Similar to (4), the bi-orthogonality between different pairs of principal vectors also holds.

2.2 Decomposition-based canonical correlation analysis

For random vectors $\{\mathbf{x}_k\}_{k=1}^2$, the D-CCA method (Shu et al., 2019) aims to decompose each \mathbf{x}_k into a common-source vector \mathbf{c}_k and a distinctive-source vector \mathbf{d}_k by

$$\mathbf{x}_k = \mathbf{c}_k + \mathbf{d}_k \quad (8)$$

subject to three desirable constraints

$$\begin{cases} \text{span}(\mathbf{c}_1^\top) = \text{span}(\mathbf{c}_2^\top), \\ \text{span}(\mathbf{d}_1^\top) \perp \text{span}(\mathbf{d}_2^\top), \\ \text{span}([\mathbf{x}_1^\top, \mathbf{x}_2^\top]) = \text{span}([\mathbf{c}_1^\top, \mathbf{c}_2^\top, \mathbf{d}_1^\top, \mathbf{d}_2^\top]). \end{cases} \quad (9)$$

To this end, guided by the bi-orthogonality (4) of augmented canonical variables $\mathbf{z}_k^\top = (z_{k1}, \dots, z_{kr_k})$ for $k \in \{1, 2\}$, D-CCA divides the decomposition problem (8) of $\text{span}([\mathbf{x}_1^\top, \mathbf{x}_2^\top])$ into r_{\max} subproblems, each within one of the mutually orthogonal subspaces $\{\text{span}(\{z_{k\ell}\}_{k=1}^2)\}_{\ell=1}^{r_{\max}}$ as

$$z_{k\ell} = c_\ell + d_{k\ell}, \quad (10)$$

where $z_{k\ell} = 0$ for $\ell > r_k$, and $c_\ell = 0$ for $\ell > r_{\min}$. For $\ell \leq r_{\min}$, the common variable c_ℓ is defined by

$$c_\ell \propto \arg \max_{w \in (\mathcal{L}_0^2, \text{cov})} \{\cos^2 \theta(z_{1\ell}, w) + \cos^2 \theta(z_{2\ell}, w)\} \quad (11)$$

such that

$$\begin{cases} d_{1\ell} \perp d_{2\ell}, \\ \|c_\ell\| \text{ increases as } \theta_{z,\ell} := \theta(z_{1\ell}, z_{2\ell}) \text{ decreases on } [0, \pi/2]. \end{cases} \quad (12)$$

$$\quad (13)$$

Constraint (13) equivalently says that $\|c_\ell\|$ indicates the correlation strength of $z_{1\ell}$ and $z_{2\ell}$. The unique solution of (11) subject to (12) and (13) is

$$c_\ell = \left(1 - \sqrt{\frac{1 - \cos \theta_{z,\ell}}{1 + \cos \theta_{z,\ell}}}\right) \frac{z_{1\ell} + z_{2\ell}}{2} = \left[1 - \tan\left(\frac{\theta_{z,\ell}}{2}\right)\right] \frac{z_{1\ell} + z_{2\ell}}{2}. \quad (14)$$

Figure 1 geometrically illustrates the solution (14) with ℓ omitted in the subscriptions.

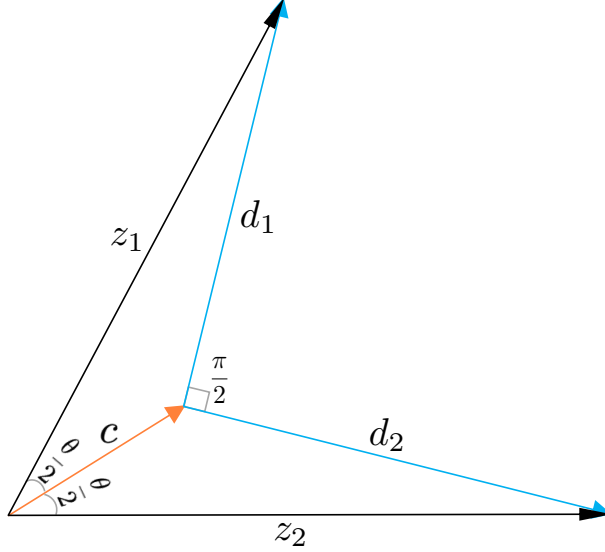


Figure 1. The geometry of D-CCA for two standardized random variables. The distinctive variables d_1 and d_2 are orthogonal (i.e., uncorrelated). The norm (i.e., standard deviation) of the common variable c indicates the correlation strength of the two standardized variables z_1 and z_2 .

Combining the solutions of subproblems yields the D-CCA decomposition: for $k = 1, 2$,

$$\mathbf{x}_k = \sum_{\ell=1}^{r_k} \beta_{k\ell} z_{k\ell} = \sum_{\ell=1}^{r_{12}} \beta_{k\ell} c_\ell + \sum_{\ell=1}^{r_k} \beta_{k\ell} d_{k\ell} =: \mathbf{c}_k + \mathbf{d}_k \quad (15)$$

with $\beta_{k\ell} = \text{cov}(\mathbf{x}_k, z_{k\ell})$. Here, $\{c_\ell\}_{\ell=1}^{r_{12}}$ are the common latent factors of \mathbf{x}_1 and \mathbf{x}_2 , and $\{d_\ell\}_{\ell=1}^{r_k}$ are the distinctive latent factors of \mathbf{x}_k . The D-CCA's decomposition structure is shown in Figure 2.

3 Common and Distinctive Pattern Analysis

The CDPA method aims to well define the common and distinctive patterns of two datasets by incorporating the common and distinctive information in the two coefficient matrices of common latent factors. We use a graph matching approach to match the unpaired rows between the coefficient matrices. Consistent estimators are established for the CDPA-defined common-pattern and distinctive-pattern matrices.

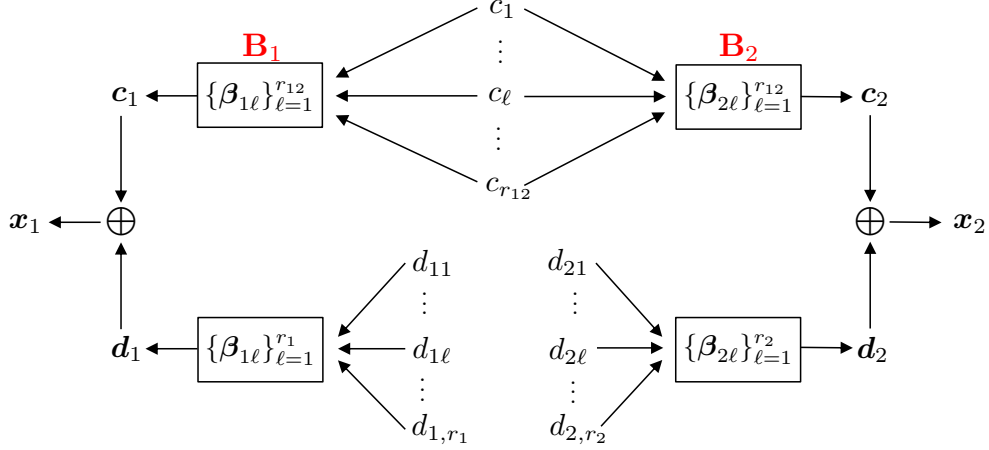


Figure 2. The D-CCA decomposition structure. D-CCA refers the common pattern of $\{\mathbf{x}_1, \mathbf{x}_2\}$ to the common latent factors $\{c_\ell\}_{\ell=1}^{r_{12}}$, but ignores the common information between their coefficient matrices $\mathbf{B}_k = (\beta_{k1}, \dots, \beta_{k,r_{12}})$ for $k = 1, 2$.

3.1 Common and distinctive patterns

As shown in Figure 2, D-CCA only focuses on the common latent factors $\{c_\ell\}_{\ell=1}^{r_{12}}$ of $\{\mathbf{x}_k\}_{k=1}^2$, and ignores the common information between their coefficient matrices $\mathbf{B}_k = (\beta_{k1}, \dots, \beta_{k,r_{12}})$ for $k = 1, 2$. In signal processing, \mathbf{B}_k is called a mixing channel (Papadias, 2000; Parra and Sajda, 2003), which introduces correlations into the uncorrelated input sources $\{c_\ell\}_{\ell=1}^{r_{12}}$ to generate the output signal \mathbf{c}_k^\top . Thus, \mathbf{B}_1 and \mathbf{B}_2 may possess common and distinctive information. In CDPA, we define a common-pattern vector \mathbf{c} for $\{\mathbf{x}_k\}_{k=1}^2$ which takes into account both the common latent sources $\{c_\ell\}_{\ell=1}^{r_{12}}$ and the common information of their mixing channels $\{\mathbf{B}_k\}_{k=1}^2$. The distinctive-pattern vector of signal \mathbf{x}_k is then defined as the residual part of the signal after removing \mathbf{c} .

In the process $\mathbf{c}_k = \mathbf{B}_k([c_\ell]_{\ell=1}^{r_{12}})^\top = \sum_{\ell=1}^{r_{12}} \beta_\ell c_\ell$, the ℓ -th column $\beta_{k\ell}$ of the mixing channel \mathbf{B}_k is the sub-channel transmitting c_ℓ , and the linear mixture of sub-channel outputs $\{\beta_\ell c_\ell\}_{\ell=1}^{r_{12}}$ reflects the “mixing” performance of the channel \mathbf{B}_k . We disentangle the common and distinctive latent structures for the two sub-channel spaces $\{\text{colsp}(\mathbf{B}_k)\}_{k=1}^2$ in a similar way as D-CCA does for the two signal spaces $\{\text{span}(\mathbf{x}_k^\top)\}_{k=1}^2$.

Two issues need to be solved before the analysis. First, the sub-channel vectors $\{\beta_{k\ell}\}_{k=2, \ell \leq r_{12}}$ may have unequal lengths p_1 and p_2 . Without loss of generality, we let $p_1 \geq p_2$ throughout the paper. When $p_1 > p_2$, we zero-pad \mathbf{B}_2 to be a $p_1 \times r_{12}$ matrix $\mathbf{B}_{2A} = [\mathbf{B}_2; \mathbf{0}_{(p_1-p_2) \times r_{12}}]$. This

zero padding is equivalent to adding $(p_1 - p_2)$ zero random variables into \mathbf{x}_2 . In other words, we are now equivalently to study the patterns between \mathbf{x}_1 and $\mathbf{x}_{2A} = [\mathbf{x}_2; \mathbf{0}_{(p_1-p_2) \times 1}]$. Second, sometimes the rows between \mathbf{B}_1 and \mathbf{B}_{2A} or equivalently the entries between \mathbf{x}_1 and \mathbf{x}_{2A} are not one-to-one matched due to their arbitrary ordering. For this scenario, we match their rows by permuting the rows of \mathbf{B}_{2A} with a permutation matrix \mathbf{P}_* . The permutation can be defined so that $\text{colsp}(\mathbf{B}_1)$ and $\text{colsp}(\mathbf{P}_* \mathbf{B}_{2A})$ are closest to each other by maximizing $\sum_{\ell=1}^{r_{12}} \cos^2 \theta_{B,\ell}$, where $\theta_{B,\ell}$ is their ℓ -th principal angle. This row-matching procedure will be discussed in detail in Section 3.2. For the generalization of our results to other row-matching criteria, we simply use an arbitrary $p_1 \times p_1$ permutation matrix \mathbf{P} in the following.

We now consider the latent structure of the two sub-channel spaces $\text{colsp}(\mathbf{B}_1)$ and $\text{colsp}(\mathbf{P} \mathbf{B}_{2A})$ by using an analogy of D-CCA on (\mathbb{R}^n, \cdot) , where constraints (8)-(13) are translated for the columns of $\{\mathbf{B}_1, \mathbf{P} \mathbf{B}_{2A}\}$ and CCA is replaced by PAA. Specifically, let $\theta_{B,\ell}$ and $\{\mathbf{v}_{B_1,\ell}, \mathbf{v}_{B_2,\ell}\}$ be the ℓ -th principal angle and the ℓ -th pair of principal vectors of $\{\text{colsp}(\mathbf{B}_1), \text{colsp}(\mathbf{P} \mathbf{B}_{2A})\}$. There are r_{12} such pairs since $\mathbf{B}_k = \mathbf{V}_k \mathbf{\Lambda}_k^{1/2} \mathbf{U}_{\theta_k}^{[:,1:r_{12}]}$ is a rank- r_{12} matrix. We define the common and distinctive components of $\{\mathbf{v}_{B_1,\ell}, \mathbf{v}_{B_2,\ell}\}$ using a decomposition similar to that in (10) and (14):

$$\mathbf{c}_{B,\ell} = \left(1 - \sqrt{\frac{1 - \cos \theta_{B,\ell}}{1 + \cos \theta_{B,\ell}}}\right) \frac{(\mathbf{v}_{B_1,\ell} + \mathbf{v}_{B_2,\ell})}{2} \quad (16)$$

and $\mathbf{d}_{B_k,\ell} = \mathbf{v}_{B_k,\ell} - \mathbf{c}_{B,\ell}$ for $k = 1, 2$ and $\ell = 1, \dots, r_{12}$. Because the principal vectors $(\mathbf{v}_{B_1,1}, \dots, \mathbf{v}_{B_1,r_{12}}) =: \mathbf{V}_{B_1}$ for $k = 1, 2$ are orthonormal bases of $\text{colsp}(\mathbf{B}_1)$ and $\text{colsp}(\mathbf{P} \mathbf{B}_{2A})$, respectively, the two channel matrices can be written as

$$\mathbf{B}_1 = \mathbf{V}_{B_1} (\mathbf{V}_{B_1}^\top \mathbf{B}_1) = ([\mathbf{c}_{B,\ell}]_{\ell=1}^{r_{12}} + [\mathbf{d}_{B_1,\ell}]_{\ell=1}^{r_{12}}) (\mathbf{V}_{B_1}^\top \mathbf{B}_1), \quad (17)$$

$$\mathbf{P} \mathbf{B}_{2A} = \mathbf{V}_{B_2} (\mathbf{V}_{B_2}^\top \mathbf{P} \mathbf{B}_{2A}) = ([\mathbf{c}_{B,\ell}]_{\ell=1}^{r_{12}} + [\mathbf{d}_{B_2,\ell}]_{\ell=1}^{r_{12}}) (\mathbf{V}_{B_2}^\top \mathbf{P} \mathbf{B}_{2A}). \quad (18)$$

The parts of \mathbf{x}_1 and $\mathbf{P} \mathbf{x}_{2A}$ that contain the common latent source variables $\{c_\ell\}_{\ell=1}^{r_{12}}$ and the common mixing-channel basis $\{\mathbf{c}_{B,\ell}\}_{\ell=1}^{r_{12}}$ are, respectively,

$$\mathbf{c}_1^* := [\mathbf{c}_{B,\ell}]_{\ell=1}^{r_{12}} \mathbf{V}_{B_1}^\top \mathbf{B}_1 ([c_\ell]_{\ell=1}^{r_{12}})^\top$$

and

$$\mathbf{c}_2^* := [\mathbf{c}_{B,\ell}]_{\ell=1}^{r_{12}} \mathbf{V}_{B_2}^\top \mathbf{P} \mathbf{B}_{2A} ([c_\ell]_{\ell=1}^{r_{12}})^\top.$$

The difference between \mathbf{c}_1^* and \mathbf{c}_2^* is the matrices $\mathbf{S}_1 := \mathbf{V}_{B_1}^\top \mathbf{B}_1$ and $\mathbf{S}_2 := \mathbf{V}_{B_2}^\top \mathbf{P} \mathbf{B}_{2A}$ in the middle of their formulas, which contain the dual weights for $\{\mathbf{c}_{B,\ell}\}_{\ell=1}^{r_{12}}$ and $\{\mathbf{c}_\ell\}_{\ell=1}^{r_{12}}$. We define the common part of the two dual weight matrices $\{\mathbf{S}_k\}_{k=1}^2$ by

$$\begin{aligned} \mathbf{S} &= \arg \min_{\mathbf{M} \in \mathbb{R}^{r_{12} \times r_{12}}} \left\| \mathbf{M} - [\text{tr}(\boldsymbol{\Sigma}_1)]^{-1/2} \mathbf{S}_1 \right\|_F^2 + \left\| \mathbf{M} - [\text{tr}(\boldsymbol{\Sigma}_2)]^{-1/2} \mathbf{S}_2 \right\|_F^2 \\ &= \frac{1}{2} \left([\text{tr}(\boldsymbol{\Sigma}_1)]^{-1/2} \mathbf{S}_1 + [\text{tr}(\boldsymbol{\Sigma}_2)]^{-1/2} \mathbf{S}_2 \right). \end{aligned} \quad (19)$$

To avoid overweighting a dataset when signals \mathbf{x}_1 and \mathbf{x}_2 have different scales, we weight \mathbf{S}_k by the scale factor $[\text{tr}(\boldsymbol{\Sigma}_k)]^{-1/2}$ in (19). This is equivalent to rescaling each \mathbf{x}_k by the factor $[\text{tr}(\boldsymbol{\Sigma}_k)]^{-1/2}$ at the very beginning as in Lock et al. (2013).

We combine the three types of common parts $\{\mathbf{c}_{B,\ell}\}_{\ell=1}^{r_{12}}$, $\{\mathbf{c}_\ell\}_{\ell=1}^{r_{12}}$ and \mathbf{S} to define the common-pattern vector of the scaled signal vectors $\mathbf{x}_1^S := [\text{tr}(\boldsymbol{\Sigma}_1)]^{-1/2} \mathbf{x}_1$ and $\mathbf{x}_2^S := [\text{tr}(\boldsymbol{\Sigma}_2)]^{-1/2} \mathbf{P} \mathbf{x}_{2A}$ as

$$\mathbf{c} = [\mathbf{c}_{B,\ell}]_{\ell=1}^{r_{12}} \mathbf{S} ([\mathbf{c}_\ell]_{\ell=1}^{r_{12}})^\top = \frac{1}{2} \left([\text{tr}(\boldsymbol{\Sigma}_1)]^{-1/2} \mathbf{c}_1^* + [\text{tr}(\boldsymbol{\Sigma}_2)]^{-1/2} \mathbf{c}_2^* \right). \quad (20)$$

For each individual unscaled signal vector \mathbf{x}_1 or $\mathbf{P} \mathbf{x}_{2A}$, we rescale \mathbf{c} to be $\mathbf{c}^{(k)} = [\text{tr}(\boldsymbol{\Sigma}_k)]^{1/2} \mathbf{c}$ and express the CDPA decomposition as

$$\mathbf{x}_k^0 = \mathbf{c}_k^0 + \mathbf{d}_k^0 =: (\mathbf{c}^{(k)} + \mathbf{h}_k) + \mathbf{d}_k^0 = \mathbf{c}^{(k)} + (\mathbf{h}_k + \mathbf{d}_k^0) =: \mathbf{c}^{(k)} + \boldsymbol{\delta}_k \quad \text{for } k = 1, 2.$$

The superscript “0” indicates to add zero padding and permutation matrix \mathbf{P} to the given vector if necessary, for example, $\mathbf{x}_1^0 = \mathbf{x}_1$ and $\mathbf{x}_2^0 = \mathbf{P} \mathbf{x}_{2A}$. For signal vector \mathbf{x}_k^0 , the vector \mathbf{h}_k represents the distinctive component within the common-source vector \mathbf{c}_k^0 , and the vector $\boldsymbol{\delta}_k$ characterizes the “total” distinctive pattern by incorporating both \mathbf{h}_k and the distinctive-source vector \mathbf{d}_k^0 . We denote $\{\mathbf{C}, \mathbf{C}^{(k)}, \mathbf{H}_k, \boldsymbol{\Delta}_k\}$ to be the corresponding sample matrices of $\{\mathbf{c}, \mathbf{c}^{(k)}, \mathbf{h}_k, \boldsymbol{\delta}_k\}$ associated with \mathbf{X}_k .

Definition 1. We define the common-pattern vector of $\{\mathbf{x}_1^0, \mathbf{x}_2^0\}$ (or more precisely, $\{\mathbf{x}_1^S, \mathbf{x}_2^S\}$) by the \mathbf{c} given in (20), and the scaled common-pattern vector for \mathbf{x}_k^0 by $\mathbf{c}^{(k)} = [\text{tr}(\boldsymbol{\Sigma}_k)]^{1/2} \mathbf{c}$. The distinctive-pattern vector of \mathbf{x}_k^0 is $\boldsymbol{\delta}_k = \mathbf{x}_k^0 - \mathbf{c}^{(k)}$. As the sample matrices of \mathbf{c} , $\{\mathbf{c}^{(k)}\}_{k=1}^2$ and $\{\boldsymbol{\delta}_k\}_{k=1}^2$, the matrices \mathbf{C} , $\{\mathbf{C}^{(k)}\}_{k=1}^2$ and $\{\boldsymbol{\Delta}_k\}_{k=1}^2$ are the common-pattern, the scaled common-pattern, and distinctive-pattern matrices of $\{\mathbf{X}_k\}_{k=1}^2$, respectively.

Theorem 1. Given any $p_1 \times p_1$ permutation matrix \mathbf{P} , the common-pattern vector \mathbf{c} defined in

(20) for $\{\mathbf{x}_1, \mathbf{P}\mathbf{x}_{2A}\}$ is unique, regardless of the non-unique choices of canonical variables $\{z_{1\ell}, z_{2\ell}\}_{\ell=1}^{r_{12}}$ and principal vectors $\{\mathbf{v}_{B_1,\ell}, \mathbf{v}_{B_2,\ell}\}_{\ell=1}^{r_{12}}$.

Remark 1. Since \mathbf{c} is the common-pattern vector of the scaled signal vectors \mathbf{x}_1^S and \mathbf{x}_2^S , $\text{tr}\{\text{cov}(\mathbf{c})\} = \text{tr}\{\text{cov}(\mathbf{c})\} / [\frac{1}{2} \sum_{k=1}^2 \text{tr}\{\text{cov}(\mathbf{x}_k^S)\}]$ represents the proportion of the average variance of \mathbf{x}_1^S and \mathbf{x}_2^S explained by \mathbf{c} , which reflects the similarity strength of the two signal vectors.

Remark 2. The common-pattern vector \mathbf{c} differs only in its sign for $\{\mathbf{x}_1, \mathbf{P}\mathbf{x}_{2A}\}$ and $\{-\mathbf{x}_1, -\mathbf{P}\mathbf{x}_{2A}\}$, but is usually quite different for $\{\mathbf{x}_1, \mathbf{P}\mathbf{x}_{2A}\}$ and $\{\mathbf{x}_1, -\mathbf{P}\mathbf{x}_{2A}\}$. We assume the sign of each entry in \mathbf{y}_k or \mathbf{x}_k cannot be arbitrarily changed, but the sign of \mathbf{y}_k or equivalently that of \mathbf{x}_k may change. The assumption is generally true if each dataset represents a data type. For example, let \mathbf{y}_2 be mRNA expression data and its entry $\mathbf{y}_2^{[i]}$ measure the mRNA expression level on the i -th gene. The arbitrary entry-wise sign changes can result in two different measurements applied to \mathbf{y}_2 . Regarding the different \mathbf{c} 's due to the sign change (if allowed) of entirely \mathbf{y}_2 or \mathbf{x}_2 , we suggest to choose the one with larger variance $\text{tr}\{\text{cov}(\mathbf{c})\}$ or, in practice, larger $\frac{1}{n} \|\widehat{\mathbf{C}}\|_F^2 = \text{tr}(\frac{1}{n} \widehat{\mathbf{C}} \widehat{\mathbf{C}}^\top)$, where $\widehat{\mathbf{C}}$ is the estimate of \mathbf{C} that will be introduced in Section 3.3. It will be shown later in Theorem 2 that $\frac{1}{n} \|\widehat{\mathbf{C}}\|_F^2 \xrightarrow{P} \text{tr}\{\text{cov}(\mathbf{c})\}$ under mild conditions. The confidence interval (CI) of $\frac{1}{n} \|\widehat{\mathbf{C}}\|_F^2$ can be constructed by bootstrapping samples (Efron and Tibshirani, 1993) once the ranks $\{r_1, r_2, r_{12}\}$ and the permutation matrix \mathbf{P} are determined.

3.2 Row matching of coefficient matrices

When the rows of coefficient matrices \mathbf{B}_1 and \mathbf{B}_{2A} are not one-to-one matched, we match them by permuting the rows of \mathbf{B}_{2A} with the following permutation matrix

$$\mathbf{P}_* = \arg \max_{\mathbf{P} \in \Pi_{p_1}} \sum_{\ell=1}^{r_{12}} \cos^2 \theta_{B,\ell},$$

where $\theta_{B,\ell}$ is the ℓ -th principal angle of $\text{colsp}(\mathbf{B}_1)$ and $\text{colsp}(\mathbf{P}\mathbf{B}_{2A})$, and Π_{p_1} is the set of all $p_1 \times p_1$ permutation matrices. By (7), this is to solve the optimization problem:

$$\mathbf{P}_* = \arg \max_{\mathbf{P} \in \Pi_{p_1}} \text{tr} \left(\mathbf{Q}_1^\top \mathbf{P} \mathbf{Q}_{2A} (\mathbf{Q}_1^\top \mathbf{P} \mathbf{Q}_{2A})^\top \right), \quad (21)$$

where $\mathbf{Q}_k \in \mathbb{R}^{p_k \times r_{12}}$ is a matrix whose columns are an orthonormal basis of $\text{colsp}(\mathbf{B}_k)$, which can be the r_{12} left singular vectors of \mathbf{B}_k , and $\mathbf{Q}_{2A} = [\mathbf{Q}_2; \mathbf{0}_{(p_1-p_2) \times r_{12}}]$ whose columns are still

an orthonormal basis of \mathbf{B}_{2A} .

The above optimization problem is equivalent to the famous graph matching problem (Lu et al., 2016). Specifically, it holds for (21) that

$$\arg \max_{\mathbf{P} \in \Pi_{p_1}} \text{tr} (\mathbf{Q}_1^\top \mathbf{P} \mathbf{Q}_{2A} (\mathbf{Q}_1^\top \mathbf{P} \mathbf{Q}_{2A})^\top) = \arg \max_{\mathbf{P} \in \Pi_{p_1}} \text{tr} (\mathbf{Q}_1 \mathbf{Q}_1^\top \mathbf{P} \mathbf{Q}_{2A} \mathbf{Q}_{2A}^\top \mathbf{P}^\top).$$

Let $\mathbf{M}_1 = \mathbf{Q}_1 \mathbf{Q}_1^\top$ and $\mathbf{M}_2 = \mathbf{Q}_{2A} \mathbf{Q}_{2A}^\top$. For $k = 1, 2$, define \mathbf{M}_k^+ to be \mathbf{M}_k if both \mathbf{M}_1 and \mathbf{M}_2 are nonnegative matrices, and otherwise let \mathbf{M}_k^+ be the matrix obtained by all elements of \mathbf{M}_k minus the smallest element of $[\mathbf{M}_1, \mathbf{M}_2]$. For any $p_1 \times p_1$ matrix \mathbf{M} , denote $\overline{\text{diag}}(\mathbf{M})$ to be the $p_1 \times p_1$ matrix having the same off-diagonal part of \mathbf{M} but with zero diagonal, and $\text{vdg}(\mathbf{M})$ to be the vector consisting of the diagonal elements of \mathbf{M} . We have

$$\begin{aligned} & \max_{\mathbf{P} \in \Pi_{p_1}} \text{tr} (\mathbf{M}_1 \mathbf{P} \mathbf{M}_2 \mathbf{P}^\top) \\ & \Leftrightarrow \min_{\mathbf{P} \in \Pi_{p_1}} \|\mathbf{M}_1 - \mathbf{P} \mathbf{M}_2 \mathbf{P}^\top\|_F^2 \\ & \Leftrightarrow \min_{\mathbf{P} \in \Pi_{p_1}} \|\mathbf{M}_1^+ - \mathbf{P} \mathbf{M}_2^+ \mathbf{P}^\top\|_F^2 \\ & \Leftrightarrow \min_{\mathbf{P} \in \Pi_{p_1}} \left\{ \|\overline{\text{diag}}(\mathbf{M}_1^+) - \mathbf{P} \overline{\text{diag}}(\mathbf{M}_2^+) \mathbf{P}^\top\|_F^2 + \|\text{vdg}(\mathbf{M}_1^+) - \mathbf{P} \text{vdg}(\mathbf{M}_2^+)\|_F^2 \right\} \\ & \Leftrightarrow \max_{\mathbf{P} \in \Pi_{p_1}} \left\{ \text{tr} (\mathbf{P}^\top \overline{\text{diag}}(\mathbf{M}_1^+) \mathbf{P} \overline{\text{diag}}(\mathbf{M}_2^+)) + \text{tr} (\mathbf{P}^\top \text{vdg}(\mathbf{M}_1^+) [\text{vdg}(\mathbf{M}_2^+)]^\top) \right\}, \quad (22) \end{aligned}$$

where the last objective function is the formula (4) of Lu et al. (2016) for the graph matching problem.

Graph matching is known to be NP-hard for the optimal solution. We use the doubly stochastic projected fixed-point (DSPFP) algorithm of Lu et al. (2016) to obtain an efficient approximation of \mathbf{P}_* , which has time complexity only $O(p_1^3)$ per iteration and space complexity $O(p_1^2)$. For ultra-large p_1 , we may further apply the approximation procedure of Olivetti et al. (2016) that employs a clustering method before DSPFP.

3.3 Estimation

Often in practice, the data matrices $\{\mathbf{Y}_k\}_{k=1}^2$ are high-dimensional and are the only observable data in decomposition (1). The literature of (1) regularly assumes high-dimensional $\{\mathbf{Y}_k\}_{k=1}^2$ to be “low-rank plus noise”. Indeed, big data matrices are often approximately low-rank in

many real-world applications (Udell and Townsend, 2019), so their low-rank approximations provide feasible or more efficient computation and meanwhile preserve the major information (Kishore Kumar and Schneider, 2017). Moreover, the low-rank plus noise structure can circumvent the curse of dimensionality (Yin et al., 1988; Koltchinskii and Lounici, 2017) in recovering the common-source and distinctive-source matrices $\{\mathbf{C}_k, \mathbf{D}_k\}_{k=1}^2$ from which our defined common-pattern and distinctive-pattern matrices are derived. Following the D-CCA paper (Shu et al., 2019), we consider the low-rank plus noise structure as follows:

$$\mathbf{Y}_k = \mathbf{X}_k + \mathbf{E}_k = \mathbf{B}_{f_k} \mathbf{F}_k + \mathbf{E}_k, \quad (23)$$

$$\mathbf{y}_k = \mathbf{x}_k + \mathbf{e}_k = \mathbf{B}_{f_k} \mathbf{f}_k + \mathbf{e}_k, \quad (24)$$

where $\mathbf{B}_{f_k} \in \mathbb{R}^{p_k \times r_k}$ is a real deterministic matrix, the columns of \mathbf{F}_k and \mathbf{E}_k are respectively the n i.i.d. copies of mean-zero random vectors \mathbf{f}_k and \mathbf{e}_k , and the vector $\mathbf{f}_k \in \mathbb{R}^{r_k}$ contains r_k latent factors such that $\text{cov}(\mathbf{f}_k) = \mathbf{I}_{r_k \times r_k}$, $\text{cov}(\mathbf{f}_k, \mathbf{e}_k) = \mathbf{0}_{r_k \times p_k}$, and $\text{span}(\mathbf{f}_k^\top)$ is a fixed subspace in $(\mathcal{L}_0^2, \text{cov})$ that is independent of $\{n, p_1, p_2\}$. Hence, r_1 , r_2 and r_{12} are fixed numbers. We can choose \mathbf{f}_k^\top to be the augmented canonical variables \mathbf{z}_k^\top . The covariance matrix $\text{cov}(\mathbf{y}_k) = \mathbf{B}_{f_k} \mathbf{B}_{f_k}^\top + \text{cov}(\mathbf{e}_k)$ is assumed to be a spiked covariance matrix for which the largest r_k eigenvalues are significantly larger than the rest, namely, signals are distinguishably stronger than noises.

Before recovering our common-pattern and distinctive-pattern matrices, we introduce the D-CCA's estimators of \mathbf{X}_k and \mathbf{C}_k . For simplicity, we write all estimators with true matrix ranks $\{r_1, r_2, r_{12}\}$. In practice, as implemented in D-CCA, ranks $\{r_k\}_{k=1}^2$ and r_{12} can be well selected by the edge distribution (ED) method of Onatski (2010) and the minimum description length information-theoretic criterion (MDL-IC) of Song et al. (2016), respectively. The estimator of \mathbf{X}_k is defined by using the soft-thresholding method of Wang and Fan (2017) as

$$\widehat{\mathbf{X}}_k = \mathbf{U}_{k1} \text{diag}(\widehat{\sigma}_1^S(\mathbf{Y}_k), \dots, \widehat{\sigma}_{r_k}^S(\mathbf{Y}_k)) \mathbf{U}_{k2}^\top, \quad (25)$$

where $\mathbf{U}_{k1} \text{diag}(\sigma_1(\mathbf{Y}_k), \dots, \sigma_{r_k}(\mathbf{Y}_k)) \mathbf{U}_{k2}^\top$ forms the top- r_k SVD of \mathbf{Y}_k , and the soft-thresholded singular value $\widehat{\sigma}_\ell^S(\mathbf{Y}_k) = \sqrt{\max\{\sigma_\ell^2(\mathbf{Y}_k) - \tau_k p_k, 0\}}$ with $\tau_k = \sum_{\ell=r_k+1}^{p_k} \sigma_\ell^2(\mathbf{Y}_k) / (np_k - nr_k - p_k r_k)$. Then from $\widehat{\mathbf{X}}_k$, define the estimator of Σ_k by $\widehat{\Sigma}_k = \frac{1}{n} \widehat{\mathbf{X}}_k \widehat{\mathbf{X}}_k^\top$, and denote its SVD by $\widehat{\Sigma}_k = \widehat{\mathbf{V}}_k \widehat{\Lambda}_k \widehat{\mathbf{V}}_k^\top$, where $\widehat{\mathbf{V}}_k \in \mathbb{R}^{p_k \times r_k}$ has orthonormal columns and $\widehat{\Lambda}_k = \text{diag}(\sigma_1(\widehat{\Sigma}_k), \dots, \sigma_{r_k}(\widehat{\Sigma}_k))$. Following Section 2.1, let $\widehat{\mathbf{Z}}_k^* = (\widehat{\Lambda}_k^\dagger)^{1/2} \widehat{\mathbf{V}}_k^\top \widehat{\mathbf{X}}_k$ and $\widehat{\Theta} = \frac{1}{n} \widehat{\mathbf{Z}}_1^* (\widehat{\mathbf{Z}}_2^*)^\top$, and write the latter's

full SVD by $\widehat{\Theta} = \widehat{\mathbf{U}}_{\theta_1} \widehat{\Lambda}_\theta \widehat{\mathbf{U}}_{\theta_2}^\top$ with $\widehat{\Lambda}_\theta = \text{diag}(\sigma_1(\widehat{\Theta}), \dots, \sigma_{\widehat{r}_\theta}(\widehat{\Theta}), \mathbf{0}_{(r_1 - \widehat{r}_\theta) \times (r_2 - \widehat{r}_\theta)})$ and $\widehat{r}_\theta = \text{rank}(\widehat{\Theta})$. Define the estimated sample matrix of \mathbf{z}_k by $\widehat{\mathbf{Z}}_k = \widehat{\mathbf{U}}_{\theta_k}^\top \widehat{\mathbf{Z}}_k^*$. Let $\widehat{\mathbf{A}}_C = \text{diag}(\widehat{a}_1, \dots, \widehat{a}_{r_{12}})$, where $\widehat{a}_\ell = \frac{1}{2} [1 - (\frac{1 - \sigma_\ell(\widehat{\Theta})}{1 + \sigma_\ell(\widehat{\Theta})})^{1/2}]$ for $\ell \leq \widehat{r}_\theta$, and otherwise $\widehat{a}_\ell = 0$. The estimator of \mathbf{C}_k is defined by

$$\widehat{\mathbf{C}}_k = \frac{1}{n} \widehat{\mathbf{X}}_k (\widehat{\mathbf{Z}}_k^{[1:r_{12},:]})^\top \widehat{\mathbf{A}}_C \sum_{j=1}^2 \widehat{\mathbf{Z}}_j^{[1:r_{12},:]} = \widehat{\mathbf{B}}_k \widehat{\mathbf{C}}_0,$$

where $\widehat{\mathbf{B}}_k = \frac{1}{n} \widehat{\mathbf{X}}_k (\widehat{\mathbf{Z}}_k^{[1:r_{12},:]})^\top = \widehat{\mathbf{V}}_k \widehat{\Lambda}_k^{1/2} \widehat{\mathbf{U}}_{\theta_k}^{[:,1:r_{12}]}$ similar to $\mathbf{B}_k = \mathbf{V}_k \Lambda_k^{1/2} \mathbf{U}_{\theta_k}^{[:,1:r_{12}]}$, and $\widehat{\mathbf{C}}_0 = \widehat{\mathbf{A}}_C \sum_{j=1}^2 \widehat{\mathbf{Z}}_j^{[1:r_{12},:]}$ is the estimated sample matrix of $(c_1, \dots, c_{r_{12}})^\top$. Matrix \mathbf{D}_k is estimated by $\widehat{\mathbf{D}}_k = \widehat{\mathbf{X}}_k - \widehat{\mathbf{C}}_k$.

We now derive the estimators of our common-pattern and distinctive-pattern matrices. Let $\widehat{\mathbf{B}}_{2A} = [\widehat{\mathbf{B}}_2; \mathbf{0}_{(p_1 - p_2) \times r_{12}}]$, $\widehat{\mathbf{Q}}_k \in \mathbb{R}^{p_k \times r_{12}}$ be the left singular matrix of $\widehat{\mathbf{B}}_k$, $\widehat{\mathbf{Q}}_{2A} = [\widehat{\mathbf{Q}}_2; \mathbf{0}_{(p_1 - p_2) \times r_{12}}]$, and $\widehat{\Theta}_B = \widehat{\mathbf{Q}}_1^\top \mathbf{P} \widehat{\mathbf{Q}}_{2A}$. We assume the permutation matrix \mathbf{P} is prespecified. If the row matching of \mathbf{B}_1 and \mathbf{B}_{2A} is necessary, one may choose \mathbf{P} to be the matrix \mathbf{P}_* in the NP-hard problem (21), approximated by the DSPFP method with data samples. Note that \mathbf{P}_* , as a permutation matrix, is either obtained exactly or approximated with at least two wrong entries. To ease theoretical analysis without such misspecification, we assume that \mathbf{P} is well determined. Write the full SVD of $\widehat{\Theta}_B$ by $\widehat{\Theta}_B = \widehat{\mathbf{U}}_{B_1} \widehat{\Lambda}_B \widehat{\mathbf{U}}_{B_2}^\top$, and define $\widehat{\mathbf{V}}_{B_1} = \widehat{\mathbf{Q}}_1 \widehat{\mathbf{U}}_{B_1}$ and $\widehat{\mathbf{V}}_{B_2} = \mathbf{P} \widehat{\mathbf{Q}}_{2A} \widehat{\mathbf{U}}_{B_2}$. It follows from (7) that the diagonal elements of $\widehat{\Lambda}_B$ and the columns of $\{\widehat{\mathbf{V}}_{B_k}\}_{k=1}^2$ are respectively the cosines of principal angles and the principal vectors of $\text{colsp}(\widehat{\mathbf{B}}_1)$ and $\text{colsp}(\mathbf{P} \widehat{\mathbf{B}}_{2A})$. Substituting them for their true counterparts in (16) yields our estimator $\widehat{\mathbf{c}}_{B,\ell}$ for $\mathbf{c}_{B,\ell}$. Then from (20), we define the estimator of \mathbf{C} by

$$\widehat{\mathbf{C}} = \frac{1}{2} [\widehat{\mathbf{c}}_{B,\ell}]_{\ell=1}^{r_{12}} \left(\widehat{\mathbf{V}}_{B_1}^\top \widehat{\mathbf{B}}_1 [\text{tr}(\widehat{\Sigma}_1)]^{-1/2} + \widehat{\mathbf{V}}_{B_2}^\top \mathbf{P} \widehat{\mathbf{B}}_{2A} [\text{tr}(\widehat{\Sigma}_2)]^{-1/2} \right) \widehat{\mathbf{C}}_0, \quad (26)$$

where $[\text{tr}(\widehat{\Sigma}_k)]^{1/2} = [\text{tr}(\frac{1}{n} \widehat{\mathbf{X}}_k \widehat{\mathbf{X}}_k^\top)]^{1/2} = \frac{1}{\sqrt{n}} \|\widehat{\mathbf{X}}_k\|_F$ estimates $[\text{tr}(\Sigma_k)]^{1/2}$. The estimator of the scaled version $\mathbf{C}^{(k)}$ is defined by

$$\widehat{\mathbf{C}}^{(k)} = [\text{tr}(\widehat{\Sigma}_k)]^{1/2} \widehat{\mathbf{C}}.$$

Given $\{r_1, r_2, r_{12}, \mathbf{P}\}$, the computational complexity of obtaining $\widehat{\mathbf{C}}$ and $\widehat{\mathbf{C}}^{(k)}$ is $O(np_1^2 \wedge n^2 p_1)$ majorly due to the SVD of $\{\mathbf{Y}_k\}_{k=1}^2$. We define the estimators $\widehat{\mathbf{H}}_k = \widehat{\mathbf{C}}_k^0 - \widehat{\mathbf{C}}^{(k)}$ and $\widehat{\Delta}_k = \widehat{\mathbf{H}}_k + \widehat{\mathbf{D}}_k^0$ for \mathbf{H}_k and Δ_k , respectively, where the superscript “0” indicates to add zero padding

and permutation matrix \mathbf{P} to the given matrix if necessary.

The following assumption given in Wang and Fan (2017) and Shu et al. (2019), which guarantees the consistency of $\{\widehat{\mathbf{X}}_k\}_{k=1}^2$, is also used to derive our asymptotic results.

Assumption 1. *We assume the following conditions for model given in (23) and (24).*

- (I) *Let $\lambda_{k1} > \dots > \lambda_{k,r_k} > \lambda_{k,r_k+1} \geq \dots \geq \lambda_{k,p_k} > 0$ be the eigenvalues of $\text{cov}(\mathbf{y}_k)$. There exist positive constants κ_1, κ_2 and δ_0 such that $\kappa_1 \leq \lambda_{k\ell} \leq \kappa_2$ for $\ell > r_k$ and $\min_{\ell \leq r_k} (\lambda_{k\ell} - \lambda_{k,\ell+1})/\lambda_{k\ell} \geq \delta_0$.*
- (II) *Assume that $p_k > \kappa_0 n$ with a constant $\kappa_0 > 0$. When $n \rightarrow \infty$, assume $\lambda_{k,r_k} \rightarrow \infty$, $p_k/(n\lambda_{k\ell})$ is upper bounded for $\ell \leq r_k$, $\lambda_{k1}/\lambda_{k,r_k}$ is bounded from above and below, and $\sqrt{p_k}(\log n)^{1/\gamma_{k2}} = o(\lambda_{r_k})$ with γ_{k2} given in (V).*
- (III) *The columns of $\mathbf{Z}_k^{(y)} := (\mathbf{\Lambda}_k^{(y)})^{-1/2}(\mathbf{V}_k^{(y)})^\top \mathbf{Y}_k$ are i.i.d. copies of $\mathbf{z}_k^{(y)} := (\mathbf{\Lambda}_k^{(y)})^{-1/2}(\mathbf{V}_k^{(y)})^\top \mathbf{y}_k$, where $\mathbf{V}_k^{(y)} \mathbf{\Lambda}_k^{(y)} (\mathbf{V}_k^{(y)})^\top$ is the full SVD of $\text{cov}(\mathbf{y}_k)$ with $\mathbf{\Lambda}_k^{(y)} = \text{diag}(\lambda_{k1}, \dots, \lambda_{k,p_k})$. The entries of $\mathbf{z}_k^{(y)}$, $z_{k1}^{(y)}, \dots, z_{k,p_k}^{(y)}$ are independent with $\mathbb{E}(z_{ki}^{(y)}) = 0$, $\text{var}(z_{ki}^{(y)}) = 1$, and the sub-Gaussian norm $\sup_{q \geq 1} q^{-1/2}(\mathbb{E}|z_{ki}^{(y)}|^q)^{1/q} \leq \kappa_s$ with a constant $\kappa_s > 0$ for all $i \leq p_k$.*
- (IV) *The matrix $\mathbf{B}_{f_k}^\top \mathbf{B}_{f_k}$ is a diagonal matrix. For all $i \leq p_k$ and $\ell \leq r_k$, $|\mathbf{B}_{f_k}^{[i,\ell]}| \leq \kappa_B \sqrt{\lambda_{k\ell}/p_k}$ with a constant $\kappa_B > 0$.*
- (V) *Denote $\mathbf{e}_k = (e_{k1}, \dots, e_{k,p_k})^\top$ and $\mathbf{f}_k = (f_{k1}, \dots, f_{k,r_k})^\top$. Assume $\|\text{cov}(\mathbf{e}_k)\|_\infty < s_0$ with a constant $s_0 > 0$. For all $i \leq p_k$ and $\ell \leq r_k$, there exist positive constants $\gamma_{k1}, \gamma_{k2}, b_{k1}$ and b_{k2} such that for $t > 0$, $\mathbb{P}(|e_{ki}| > t) \leq \exp(-(t/b_{k1})^{\gamma_{k1}})$ and $\mathbb{P}(|f_{k\ell}| > t) \leq \exp(-(t/b_{k2})^{\gamma_{k2}})$.*

Theorem 2. *Suppose that Assumption 1 and $r_{12} \geq 1$ hold. Assume that any distinct values in $\{\cos \theta_{B,\ell}\}_{\ell=1}^{r_{12}} \cup \{0, -\infty\}$ are separated by at least a positive constant. Define*

$$\delta_\theta = \left(\frac{1}{\sqrt{n}} + \sum_{k=1}^2 \sqrt{\frac{p_k \log p_k}{n R_k}} \right) \wedge 1$$

with $R_k = \lambda_{r_k}(\text{cov}(\mathbf{x}_k))/\lambda_1(\text{cov}(\mathbf{e}_k))$. For $k = 1, 2$, we have that

$$\frac{\|\widehat{\mathbf{C}} - \mathbf{C}\|_*^2}{\frac{1}{2}(\|\mathbf{X}_1^S\|_*^2 + \|\mathbf{X}_2^S\|_*^2)} \vee \frac{\|\widehat{\mathbf{C}}^{(k)} - \mathbf{C}^{(k)}\|_*^2}{\|\mathbf{X}_k\|_*^2} = O_P(\delta_\theta)$$

and

$$\left| \operatorname{tr}\left(\frac{1}{n}\widehat{\mathbf{C}}\widehat{\mathbf{C}}^\top\right) - \operatorname{tr}\{\operatorname{cov}(\mathbf{c})\} \right| = O_P(\delta_\theta^{1/2}),$$

where $\|\cdot\|_*$ denotes either the Frobenius norm or the spectral norm, and $\mathbf{X}_k^S = [\operatorname{tr}(\boldsymbol{\Sigma}_k)]^{-1/2}\mathbf{X}_k$.

Remark 3. From Theorem 3 and Corollary 1 of Shu et al. (2019), we have $\|\widehat{\mathbf{M}}_k - \mathbf{M}_k\|_*^2 / \|\mathbf{X}_k\|_*^2 = O_P(\delta_\theta)$ for $\mathbf{M}_k \in \{\mathbf{X}_k, \mathbf{C}_k, \mathbf{D}_k\}$. Additionally by our Theorem 2 and the triangle inequality of norms, we also have such scaled squared errors for $\mathbf{M}_k \in \{\mathbf{H}_k, \boldsymbol{\Delta}_k\}$. Note that the scaled squared error in the Frobenius norm indicates the scaled loss in matrix variation (sum of squares).

Theorem 3. Let $\widehat{\mathbf{P}}_* = \arg \max_{\mathbf{P} \in \Pi_{p_1}} \operatorname{tr}(\widehat{\mathbf{Q}}_1^\top \mathbf{P} \widehat{\mathbf{Q}}_{2A} (\widehat{\mathbf{Q}}_1^\top \mathbf{P} \widehat{\mathbf{Q}}_{2A})^\top)$. Suppose that Assumption 1 and $r_{12} \geq 1$ hold. Then, we have

$$\left| \operatorname{tr}(\mathbf{Q}_1^\top \widehat{\mathbf{P}}_* \mathbf{Q}_{2A} (\mathbf{Q}_1^\top \widehat{\mathbf{P}}_* \mathbf{Q}_{2A})^\top) - \operatorname{tr}(\mathbf{Q}_1^\top \mathbf{P}_* \mathbf{Q}_{2A} (\mathbf{Q}_1^\top \mathbf{P}_* \mathbf{Q}_{2A})^\top) \right| = O_P(\delta_\theta).$$

For the row matching problem of \mathbf{B}_1 and \mathbf{B}_{2A} , Theorem 3 provides an asymptotically vanishing bound on the change in the objective function value of (21) when the optimal solution \mathbf{P}_* is replaced by $\widehat{\mathbf{P}}_*$.

4 Simulation Studies

We consider the following two simulation setups to evaluate the finite-sample performance of our proposed estimators and examine our asymptotic results given in Section 3.3.

Setup 1: We set the dimensions $p_1 = p_2$, ranks $r_1 = r_2 = 5$, and eigenvalues $\lambda_\ell(\boldsymbol{\Sigma}_k) = 500 - 100(\ell - 1)$ for $\ell \leq 5$. The signals are $\mathbf{x}_k = \mathbf{V}_k \boldsymbol{\Lambda}_k^{1/2} \mathbf{z}_k$ for $k = 1, 2$, where canonical variables $(\mathbf{z}_1^\top, \mathbf{z}_2^\top)^\top$ follow a multivariate Gaussian distribution with $\mathbf{z}_k \sim \mathcal{N}(\mathbf{0}_{r_k \times 1}, \mathbf{I}_{r_k \times r_k})$ and $\operatorname{cov}(\mathbf{z}_1, \mathbf{z}_2) = \operatorname{diag}\{\cos(\theta \wedge 30^\circ), \cos(\theta \wedge 60^\circ), \cos \theta, \cos(\theta + 15^\circ), \cos((\theta + 30^\circ) \wedge 90^\circ)\}$. Let $\mathbf{Q}_k = \mathbf{V}_k^{[:,1:r_{12}]}$, $\mathbf{P} = \mathbf{I}_{p_1 \times p_1}$, and $\mathbf{Q}_1^\top \mathbf{Q}_2 = \operatorname{cov}(\mathbf{z}_1, \mathbf{z}_2)^{[1:r_{12}, 1:r_{12}]}$ where the diagonal contains the cosines of principal angles of $\operatorname{colsp}(\mathbf{B}_1)$ and $\operatorname{colsp}(\mathbf{B}_{2A})$. Matrices $\{\mathbf{V}_k\}_{k=1}^2$ are randomly generated under the above constraints and are fixed for all replications. Noises $\{e_{ki}\}_{k \leq 2, i \leq p_k} \stackrel{i.i.d.}{\sim} \mathcal{N}(0, \sigma_e^2)$ are independent of $\{\mathbf{x}_k\}_{k=1}^2$. We vary p_1 from 100 to 1500, θ from 0° to 75° , and σ_e^2 from 0.01 to 16.

Setup 2: We vary p_1 but fix $p_2 = 900$. The other settings are the same as those in Setup 1. This setup aims to evaluate our proposed estimation when $p_1 \neq p_2$.

Each simulation setup was implemented with sample size $n = 300$ and 1000 replications. Same for all p_1 values, the proportion of the average variance of \mathbf{x}_1^S and \mathbf{x}_2^S explained by \mathbf{c} , that is, $\text{tr}\{\text{cov}(\mathbf{c})\}$, has values 0.890, 0.479, 0.213, 0.126, 0.092, and 0.088 corresponding to θ from 0° to 75° by a step 15° . The noise variance $\sigma_e^2 = \lambda_1(\text{cov}(\mathbf{e}_k))$ and the resulting signal-to-noise eigenratio $R_k = 100/\sigma_e^2$. The noise levels according to different σ_e^2 values are illustrated in Figure 3, as compared to two random replications of signal matrix \mathbf{X}_1 with dimension $p_1 = 300$ and $p_1 = 900$. We see that the signal matrix \mathbf{X}_1 is overwhelmed by noises when $\sigma_e^2 \geq 4$. We used the true $\{r_k\}_{k=1}^2$, r_{12} , and \mathbf{P} in our estimation here to exclude the error induced by their misspecification. Those parameters can be selected in practice by the ED, MDL-IC, and DSPFP methods, respectively.

We first investigate the performance of our common-pattern matrix estimator $\widehat{\mathbf{C}}$ defined in (26). Figure 4 shows the scaled squared errors of $\widehat{\mathbf{C}}$ as studied in Theorem 2 and its relative squared errors under Setup 1. These squared errors in the Frobenius norm represent the scaled

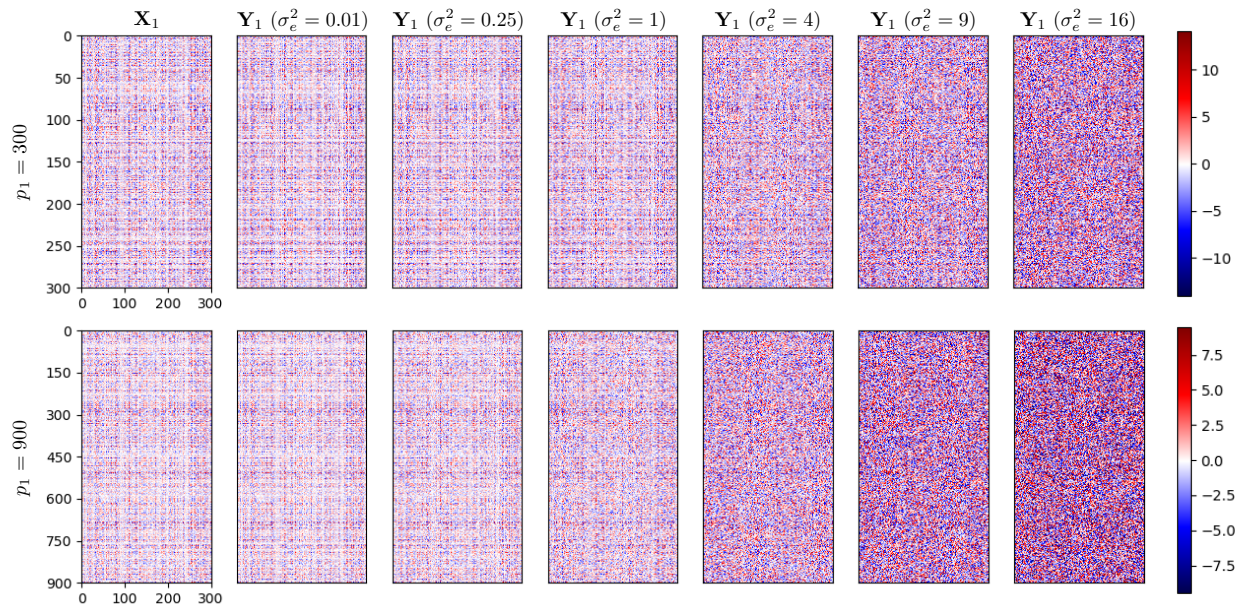


Figure 3. An illustration of noise levels in simulation setups. Each colorbar shows values ranging from the corresponding $-\|\mathbf{X}_1\|_{\max}$ to $\|\mathbf{X}_1\|_{\max}$. The signal matrix \mathbf{X}_1 is overwhelmed by noises when $\sigma_e^2 \geq 4$.

or relative losses in matrix variation (sum of squares). The estimation errors increase as the noise variance $\sigma_e^2 = 100/R_k$ or the dimension p_1 grows, and are even well controlled under 0.1 for many cases with large $\sigma_e^2 \geq 4$ and large $p_1 \geq 900$. These results are consistent with the influence of p_1 and R_k on the convergence rates given in Theorem 2. Similar numerical results are observed for the scaled version $\widehat{\mathbf{C}}^{(k)} = [\text{tr}(\widehat{\boldsymbol{\Sigma}}_k)]^{1/2} \widehat{\mathbf{C}}$ and the distinctive-pattern matrix estimator $\widehat{\boldsymbol{\Delta}}_k = \widehat{\mathbf{X}}_k - \widehat{\mathbf{C}}^{(k)}$ for $k \in \{1, 2\}$, and hence are omitted for brevity.

As an indicator for the similarity strength of signals \mathbf{x}_1 and \mathbf{x}_2 , the common-pattern explained proportion of signal variance, $\text{tr}\{\text{cov}(\mathbf{c})\}$, is estimated by $\text{tr}(\frac{1}{n} \widehat{\mathbf{C}} \widehat{\mathbf{C}}^\top) = \frac{1}{n} \|\widehat{\mathbf{C}}\|_F^2$. Figure 5 plots the absolute error and relative error of this estimator for Setup 1. Same with Theorem 2, the figure shows that the estimation errors grow with increasing p_1 or σ_e^2 and have a larger magnitude than those squared errors of $\widehat{\mathbf{C}}$ as shown in Figure 4. The relative errors are controlled below 0.1 even for some cases with large p_1 or σ_e^2 values.

For the row matching approach of coefficient matrices $\{\mathbf{B}_k\}_{k=1}^2$ described in Section 3.2, its theoretical performance stated in Theorem 3 is numerically investigated with the intractable \mathbf{P}_* and $\widehat{\mathbf{P}}_*$ being replaced by their DSPFP approximations denoted as \mathbf{P}_a and $\widehat{\mathbf{P}}_a$. Figure 6 displays the absolute and relative errors of $\text{tr}(\mathbf{Q}_1^\top \widehat{\mathbf{P}}_a \mathbf{Q}_{2A} (\mathbf{Q}_1^\top \widehat{\mathbf{P}}_a \mathbf{Q}_{2A})^\top)$ for Setup 1. Although its absolute errors seem to have larger values than what are expected for those of its oracle version (with $\widehat{\mathbf{P}}_*$) given in Theorem 3, its relative errors are controlled under or around 0.1 even for some cases with large $p_1 \geq 900$ or $\sigma_e^2 \geq 4$, and moreover, the two types of errors both follow the influence of p_1 and $R_k (= 100/\sigma_e^2, \text{ here})$ on the convergence rate shown in the theorem.

The above result patterns also generally hold for settings with more different values of θ (or equivalently $\text{tr}\{\text{cov}(\mathbf{c})\}$) and for those under Setup 2 where $p_1 \neq p_2$, which are provided in the Supplementary Material.

5 Real Data Examples

5.1 Application to HCP motor-task functional MRI data

We consider the HCP motor-task functional MRI data obtained from 1080 healthy young adults (Barch et al., 2013). All participants were asked by visual cues to perform five motor tasks during the image scanning, including tapping left and right fingers, squeezing left and right toes, and

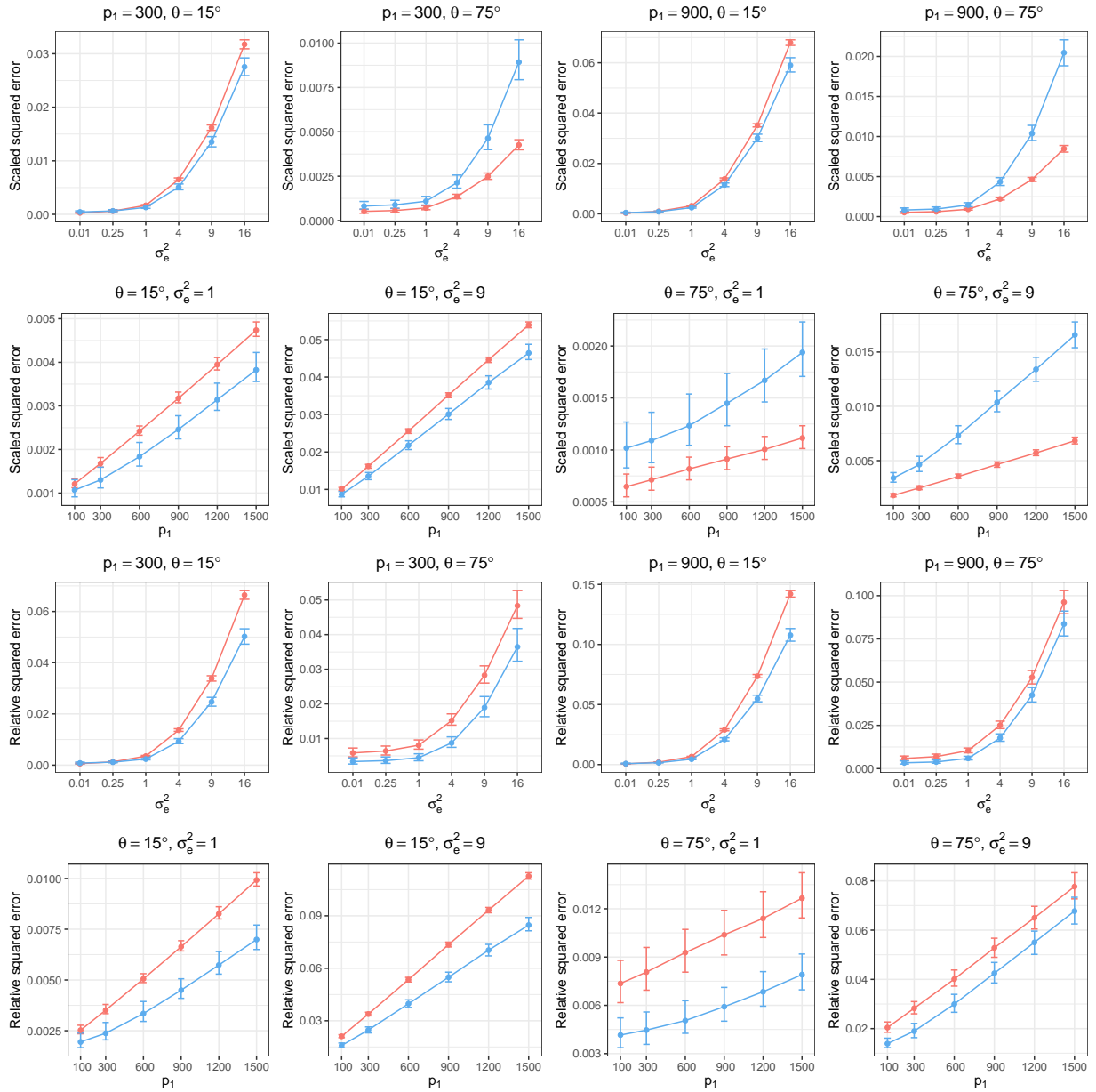


Figure 4. Simulation results for Setup 1: medians and interquartile ranges of the scaled squared error $2\|\hat{\mathbf{C}} - \mathbf{C}\|_*^2 / (\|\mathbf{X}_1^S\|_*^2 + \|\mathbf{X}_2^S\|_*^2)$ and the relative squared error $\|\hat{\mathbf{C}} - \mathbf{C}\|_*^2 / \|\mathbf{C}\|_*^2$ over 1000 replications in the Frobenius norm (red) and the spectral norm (blue).

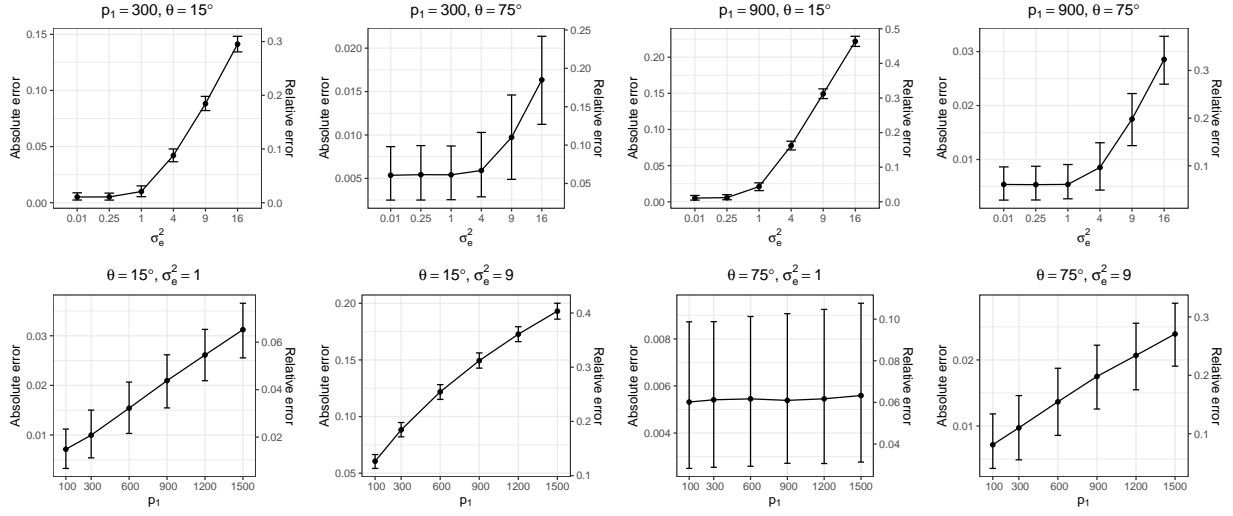


Figure 5. Simulation results for Setup 1: medians and interquartile ranges of the absolute error $|\text{tr}(\frac{1}{n}\widehat{\mathbf{C}}\widehat{\mathbf{C}}^\top) - \text{tr}\{\text{cov}(\mathbf{c})\}|$ and the relative error $|\text{tr}(\frac{1}{n}\widehat{\mathbf{C}}\widehat{\mathbf{C}}^\top)/\text{tr}\{\text{cov}(\mathbf{c})\} - 1|$ over 1000 replications.

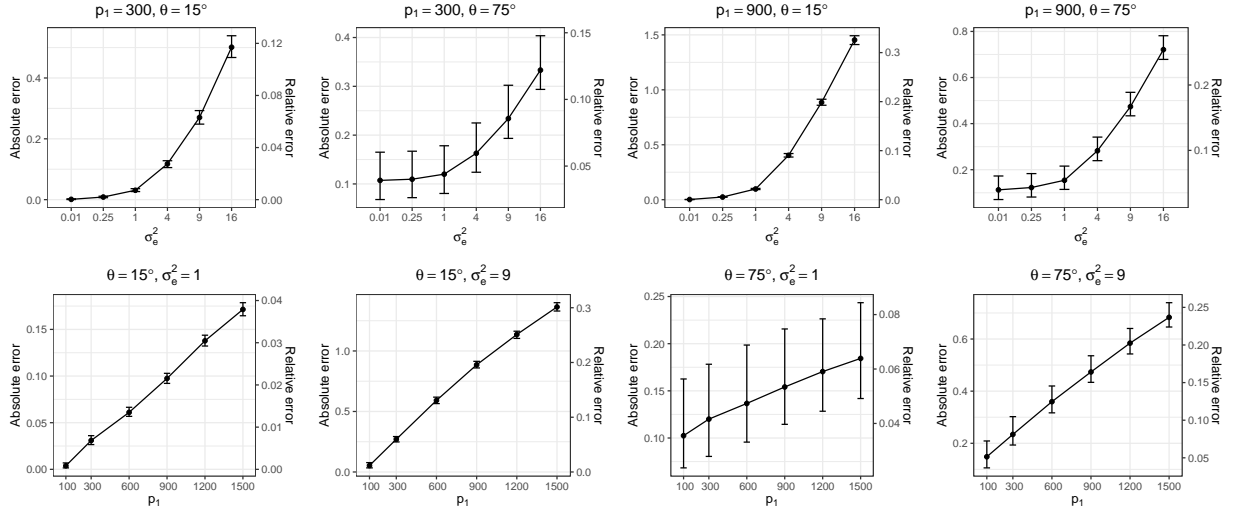


Figure 6. Simulation results for Setup 1: medians and interquartile ranges of the absolute error $|\text{tr}(\mathbf{Q}_1^\top \widehat{\mathbf{P}}_a \mathbf{Q}_{2A} (\mathbf{Q}_1^\top \widehat{\mathbf{P}}_a \mathbf{Q}_{2A})^\top) - \text{tr}(\mathbf{Q}_1^\top \mathbf{P}_a \mathbf{Q}_{2A} (\mathbf{Q}_1^\top \mathbf{P}_a \mathbf{Q}_{2A})^\top)|$ and the relative error $|\text{tr}(\mathbf{Q}_1^\top \widehat{\mathbf{P}}_a \mathbf{Q}_{2A} (\mathbf{Q}_1^\top \widehat{\mathbf{P}}_a \mathbf{Q}_{2A})^\top) / \text{tr}(\mathbf{Q}_1^\top \mathbf{P}_a \mathbf{Q}_{2A} (\mathbf{Q}_1^\top \mathbf{P}_a \mathbf{Q}_{2A})^\top) - 1|$ over 1000 replications.

moving tongue. From the acquired brain images, for every participant and each task, the HCP computed a z -statistic map of the task’s contrast against the fixation baseline at 91,282 grayordinates including 59,412 cortical surface vertices and 31,870 subcortical gray matter voxels. The z -statistic maps of all participants for each individual task constitute a $91,282 \times 1080$ data matrix. We focus on the left-hand and right-hand tasks, and apply proposed CDPA method to discover their common pattern on the brain, with comparison to the state-of-the-art D-CCA.

Each of the two observed data matrices is row-centered by subtracting the average within each row. Since all z -statistic maps of the two motor tasks are obtained from the same measurement and at the same set of grayordinates, there is no need to choose the signs or match the rows of the two data matrices. We consider the variance maps of $\{\mathbf{x}_L, \mathbf{x}_R, \mathbf{c}_L, \mathbf{c}_R, \mathbf{c}\}$ on the brain, which are estimated by the sample variances computed from the estimated sample matrices $\{\widehat{\mathbf{X}}_L, \widehat{\mathbf{X}}_R, \widehat{\mathbf{C}}_L, \widehat{\mathbf{C}}_R, \widehat{\mathbf{C}}\}$ obtained by D-CCA and CDPA. Here, the subscripts L and R denote the left-hand and right-hand tasks. The ranks $\{r_L, r_R\}$ and r_{12} are all selected as two by the ED and MDL-IC methods, respectively. The proportions of corresponding signal variances explained by common-source vectors \mathbf{c}_L and \mathbf{c}_R are $\frac{\text{tr}\{\text{cov}(\mathbf{c}_L)\}}{\text{tr}\{\text{cov}(\mathbf{x}_L)\}} \approx \frac{\|\widehat{\mathbf{C}}_L\|_F^2}{\|\widehat{\mathbf{X}}_L\|_F^2} = 0.113$ and $\frac{\text{tr}\{\text{cov}(\mathbf{c}_R)\}}{\text{tr}\{\text{cov}(\mathbf{x}_R)\}} \approx \frac{\|\widehat{\mathbf{C}}_R\|_F^2}{\|\widehat{\mathbf{X}}_R\|_F^2} = 0.111$. The common-pattern explained proportion of signal variance is $\text{tr}\{\text{cov}(\mathbf{c})\} \approx \frac{1}{n} \|\widehat{\mathbf{C}}\|_F^2 = 0.077$.

Figure 7 presents the estimated variance maps. For all the five maps, the estimated variances of cortical surface vertices overall dominate those of subcortical voxels. We hence focus on the part of each variance map for the cortical surface. From the estimated signal variance maps $\widehat{\text{var}}(\mathbf{x}_L)$ and $\widehat{\text{var}}(\mathbf{x}_R)$ shown in Figure 7 (a) and (b), we see that the right half brain is more active, with larger variances, on the cortical surface for the left-hand task, while the pattern is almost opposite for the right-hand task. In particular, the contralateral pattern is clearly seen on the somatomotor cortex annotated by green circles, a brain region known to be linked with hand tasks (Buckner et al., 2011). A similar contralateral pattern is also observed for $\widehat{\text{var}}(\mathbf{c}_L)$ and $\widehat{\text{var}}(\mathbf{c}_R)$ in Figure 7 (c) and (d). This indicates that the \mathbf{c}_k vector of D-CCA remains some distinctive pattern of \mathbf{x}_k for $k \in \{L, R\}$. It is not surprising because \mathbf{c}_L and \mathbf{c}_R have different coefficient matrices of the common latent factors, which are r_{12} columns in the coefficient matrices of canonical variables for \mathbf{x}_L and \mathbf{x}_R , respectively, as shown in equation (15). In contrast, our CDPA’s common-pattern vector \mathbf{c} in Figure 7 (e) has an estimated variance map that is nearly

symmetric on the two hemispheres, and thus is more reasonable than D-CCA's common-source vectors $\{c_k\}_{k \in \{L,R\}}$ to represent the common pattern of the left-hand and right-hand tasks on the brain.

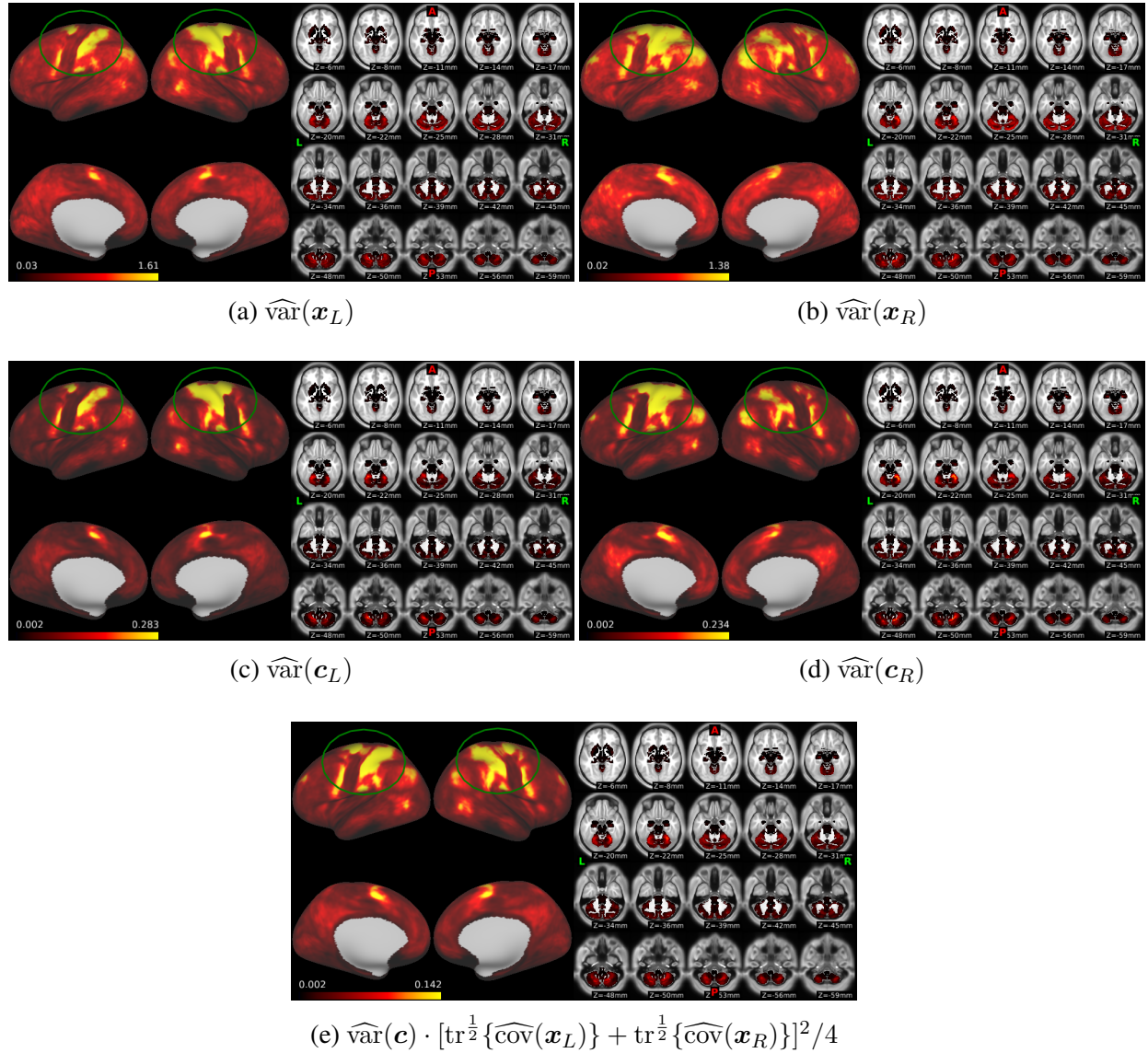


Figure 7. The estimated variance maps for HCP motor-task functional MRI data. The notations $\widehat{\text{var}}$ and $\widehat{\text{cov}}$ denote the sample variance vector and sample covariance matrix obtained from the corresponding recovered sample matrix. In each subfigure, the left part displays the cortical surface with the outer side shown in the first row and the inner side in the second row; the right part shows the subcortical area on 20 xy slides at the z axis. The somatomotor cortex is annotated by green circles.

5.2 Application to TCGA breast cancer genomic datasets

With the aim to discover new breast cancer subtypes, we apply the proposed CDPA method to two TCGA breast cancer genomic datasets (Koboldt et al., 2012), and compare the results with the D-CCA method. We consider the DNA methylation data and mRNA expression data obtained from a common set of 703 tumor samples. Following the preprocessing procedure of Lock and Dunson (2013), we select the top 1100 variable probes for the DNA methylation dataset and the top 896 variably expressed genes for the mRNA expression dataset. The tumor samples are categorized by the classic PAM50 model (Parker et al., 2009) into four intrinsic subtypes, including 124 Basal-like, 58 HER2-enriched, 348 Luminal A, and 173 Luminal B tumors.

The two data matrices of interest have sizes 1100×703 and 896×703 , respectively, and are row-centered before analysis. The ranks $(r_{\text{DNA}}, r_{\text{mRNA}}, r_{12})$ are selected by the ED and MDL-IC methods as $(3, 2, 2)$. From the D-CCA, the proportions of signal variances explained by common-source vectors \mathbf{c}_{DNA} and \mathbf{c}_{mRNA} are $\frac{\text{tr}\{\text{cov}(\mathbf{c}_{\text{DNA}})\}}{\text{tr}\{\text{cov}(\mathbf{x}_{\text{DNA}})\}} \approx \frac{\|\widehat{\mathbf{C}}_{\text{DNA}}\|_F^2}{\|\widehat{\mathbf{X}}_{\text{DNA}}\|_F^2} = 0.210$ and $\frac{\text{tr}\{\text{cov}(\mathbf{c}_{\text{mRNA}})\}}{\text{tr}\{\text{cov}(\mathbf{x}_{\text{mRNA}})\}} \approx \frac{\|\widehat{\mathbf{C}}_{\text{mRNA}}\|_F^2}{\|\widehat{\mathbf{X}}_{\text{mRNA}}\|_F^2} = 0.422$, respectively, indicating the different influence of the common underlying mechanism on each signal dataset. Thus, their \mathbf{c}_{DNA} and \mathbf{c}_{mRNA} are not appropriate to be viewed as the common pattern of \mathbf{x}_{DNA} and \mathbf{x}_{mRNA} .

Since the rows of either observed data matrix can be arbitrarily ordered independent of the other matrix, before implementing CDPA we match their rows using the graph-matching based approach described in Section 3.2. The CDPA method shows that the common-pattern explained proportion of signal variance $\text{tr}\{\text{cov}(\mathbf{c})\} \approx \frac{1}{n} \|\widehat{\mathbf{C}}\|_F^2$ is 0.161 (95% CI = [0.154, 0.185]) for \mathbf{x}_{DNA} and \mathbf{x}_{mRNA} , but is only 0.049 (95% CI = [0.046, 0.057]) for \mathbf{x}_{DNA} and $-\mathbf{x}_{\text{mRNA}}$, where each 95% CI is computed by 5000 bootstrapping samples. We hence focus on the common and distinctive patterns extracted from $\{\mathbf{x}_{\text{DNA}}, \mathbf{x}_{\text{mRNA}}\}$ rather than $\{\mathbf{x}_{\text{DNA}}, -\mathbf{x}_{\text{mRNA}}\}$.

We explore new cancer subtypes by conducting clustering analysis on each observed or recovered matrix from the CDPA and D-CCA methods. We use the Ward’s hierarchical clustering method (Ward, 1963) with the Euclidean distance, and simply specify the number of clusters to be four, which is the same number of the PAM50 intrinsic subtypes.

Table 1 compares the differences in survival curves of identified clusters or given subtypes using two most popular methods, the log-rank test (Mantel, 1966; Cox, 1972) and the Peto-Peto’s Wilcoxon test (Peto and Peto, 1972), where the latter test is more sensitive to early survival dif-

ferences. Our CDPA's $\widehat{\Delta}_{\text{mRNA}}$ -identified clusters and the PAM50 intrinsic subtypes both have very significantly distinct survival behaviors with the two smallest p-values below 0.003 in both tests, while the other matrices generate much less pronounced clusters, in particular, the matrices $\{\mathbf{C}_k, \mathbf{D}_k\}_{k \in \{\text{DNA}, \text{mRNA}\}}$ of D-CCA all have large p-values greater than 0.29. By comparing the p-values of $\widehat{\mathbf{C}}$, $\widehat{\mathbf{X}}_k$ and $\widehat{\Delta}_k$ for each k , the improved discriminative power of distinctive-pattern matrix estimate $\widehat{\Delta}_k$ can be attributed to removing the less sensitive common-pattern matrix estimate $\widehat{\mathbf{C}}$ from the denoised data matrix $\widehat{\mathbf{X}}_k$.

We match the $\widehat{\Delta}_{\text{mRNA}}$ -identified clusters with PAM50 subtypes by reordering their matching matrix such that its diagonal sum is maximized. The resulting Cohen's kappa coefficient is only 0.414 (95% CI = [0.365, 0.463]), indicating their agreement strength on the boundary of the fair and moderate levels in the criterion of Landis and Koch (1977).

Let $\widehat{\Delta}_{\text{mRNA}}-i$ denote the i -th cluster identified from $\widehat{\Delta}_{\text{mRNA}}$. Figure 8 displays the Kaplan-Meier survival curves of $\widehat{\Delta}_{\text{mRNA}}$ -identified clusters and PAM50 subtypes. With the worst survival curve among the four identified clusters, $\widehat{\Delta}_{\text{mRNA}}-4$ behaves similar to the HER2-enriched subtype, but is notably different with all other identified clusters and intrinsic subtypes. This is further confirmed in Table 2 by the minimum p-value of corresponding log-rank test and Peto-Petos Wilcoxon test with the significance level set as 0.05. Also seen in the table, the first three $\widehat{\Delta}_{\text{mRNA}}$ -identified clusters have no significant survival differences with large p-values. Moreover, the matching matrix in Table 3 shows that most of $\widehat{\Delta}_{\text{mRNA}}-1$ and $\widehat{\Delta}_{\text{mRNA}}-2$ samples belong to the Basal-like and Luminal A subtypes, respectively. Hence, the first three $\widehat{\Delta}_{\text{mRNA}}$ -identified clusters are less of interest to be new subtypes, and we focus on $\widehat{\Delta}_{\text{mRNA}}-4$ which has the poorest survival, and further compare it with the HER2-enriched subtype.

From Table 3, we see that the $\widehat{\Delta}_{\text{mRNA}}-4$ cluster (97 samples) and the HER2-enriched subtype (58 samples) share only 7 samples and have substantially distinct clinical features in terms of the three important receptors' status. In particular, the $\widehat{\Delta}_{\text{mRNA}}-4$ cluster primarily includes those samples that are ER+ and/or PR+, whereas the HER2-enriched subtype contains those that are HER2+ and/or PR-. To conclude, the $\widehat{\Delta}_{\text{mRNA}}-4$ cluster, with low survival rate, is remarkably different from the four PAM50 subtypes and appears to be an important new breast cancer subtype worthy further investigation.

Table 1. Log-rank test and Peto-Peto's Wilcoxon test for survival curve differences among the clusters identified from each matrix of TCGA breast cancer datasets.

Data	Log-rank/Peto's p-values	Data	Log-rank/Peto's p-values	Data	Log-rank/Peto's p-values
\widehat{Y}_{DNA}	0.175/0.230	\widehat{Y}_{mRNA}	0.251/0.299	$[\widehat{Y}_{DNA}^N; \widehat{Y}_{mRNA}^N]$	0.245/0.129
\widehat{X}_{DNA}	0.077/0.112	\widehat{X}_{mRNA}	0.063/0.061	$[\widehat{X}_{DNA}^N; \widehat{X}_{mRNA}^N]$	0.565/0.619
\widehat{C}_{DNA}	0.820/0.979	\widehat{C}_{mRNA}	0.619/0.704	$[\widehat{C}_{DNA}^N; \widehat{C}_{mRNA}^N]$	0.752/0.751
\widehat{D}_{DNA}	0.515/0.417	\widehat{D}_{mRNA}	0.290/0.354	$[\widehat{D}_{DNA}^N; \widehat{D}_{mRNA}^N]$	0.149/0.223
\widehat{H}_{DNA}	0.430/0.502	\widehat{H}_{mRNA}	0.330/0.409	$[\widehat{H}_{DNA}^N; \widehat{H}_{mRNA}^N]$	0.337/0.369
$\widehat{\Delta}_{DNA}$	0.058/0.075	$\widehat{\Delta}_{mRNA}$	5.08e-4/1.27e-3	$[\widehat{\Delta}_{DNA}^N; \widehat{\Delta}_{mRNA}^N]$	0.218/0.208
\widehat{C}	0.106/0.163	PAM50	2.62e-3/1.13e-3		

Note: Denote $M^N = M/\|M\|_F$ for any matrix M .

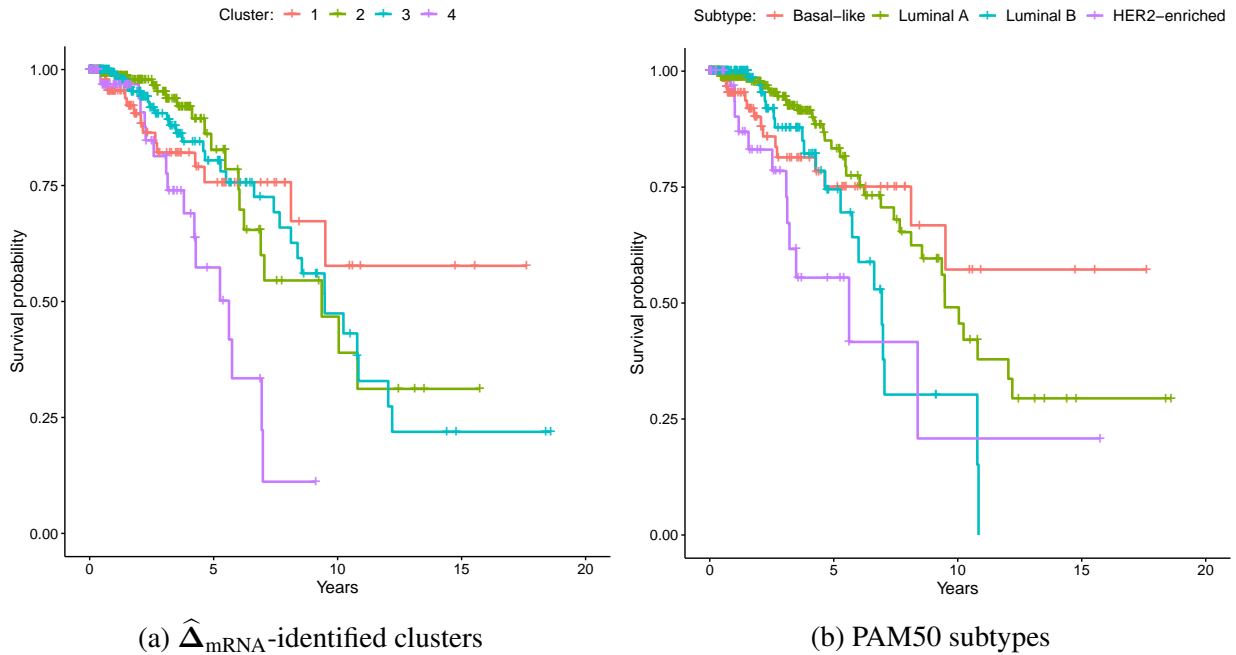


Figure 8. Kaplan-Meier survival curves of TCGA breast cancer clusters and subtypes.

Table 2. Log-rank test and Peto-Peto’s Wilcoxon test for survival curve differences among $\widehat{\Delta}_{\text{mRNA}}$ -identified clusters and PAM50 subtypes for TCGA breast cancer data analysis.

Comparison	Log-rank/Peto’s p-values	Comparison	Log-rank/Peto’s p-values
$\widehat{\Delta}_{\text{mRNA}}-1$ vs. $\widehat{\Delta}_{\text{mRNA}}-2$	0.751/0.430	$\widehat{\Delta}_{\text{mRNA}}-1$ vs. $\widehat{\Delta}_{\text{mRNA}}-3$	0.781/0.823
$\widehat{\Delta}_{\text{mRNA}}-1$ vs. $\widehat{\Delta}_{\text{mRNA}}-4$	0.012/0.043	$\widehat{\Delta}_{\text{mRNA}}-2$ vs. $\widehat{\Delta}_{\text{mRNA}}-3$	0.585/0.589
$\widehat{\Delta}_{\text{mRNA}}-2$ vs. $\widehat{\Delta}_{\text{mRNA}}-4$	1.30e-4/1.50e-4	$\widehat{\Delta}_{\text{mRNA}}-3$ vs. $\widehat{\Delta}_{\text{mRNA}}-4$	3.70e-4/9.50e-4
$\widehat{\Delta}_{\text{mRNA}}-4$ vs. Basal-like	0.015/0.053	$\widehat{\Delta}_{\text{mRNA}}-4$ vs. Luminal A	8.10e-6/1.64e-5
$\widehat{\Delta}_{\text{mRNA}}-4$ vs. Luminal B	0.031/0.028	$\widehat{\Delta}_{\text{mRNA}}-4$ vs. HER2-enriched	0.820/0.571

Table 3. Matching matrix and clinical features of $\widehat{\Delta}_{\text{mRNA}}$ -identified clusters and PAM50 subtypes for TCGA breast cancer data analysis.

PAM50	$\widehat{\Delta}_{\text{mRNA}}-1$	$\widehat{\Delta}_{\text{mRNA}}-2$	$\widehat{\Delta}_{\text{mRNA}}-3$	$\widehat{\Delta}_{\text{mRNA}}-4$	Total	ER+/-	PR+/-	HER2+/-
Basal-like	123	0	1	0	124	6%/81%	6%/79%	7%/54%
Luminal A	0	188	134	26	348	89%/1%	82%/8%	9%/53%
Luminal B	0	18	91	64	173	87%/2%	72%/17%	16%/46%
HER2-enriched	9	9	33	7	58	33%/52%	17%/71%	62%/16%
Total	132	215	259	97	703			
ER+/-	6%/80%	92%/3%	78%/9%	84%/2%				
PR+/-	6%/79%	83%/11%	67%/20%	67%/19%				
HER2+/-	10%/52%	11%/56%	20%/41%	18%/44%				

Notes: The columns of the matching matrix are well reordered such that its diagonal sum is maximized. Receptor status for estrogen (ER), progesterone (PR) and human epidermal growth factor 2 (HER2) includes positive (+), negative (-), and N/A or equivocal.

Supplementary Materials

The Supplementary Materials include all theoretical proofs in in Section S.1 and additional simulation results in Section S.2.

S.1 Theoretical Proofs

Proof of Theorem 1. For $k = 1, 2$, denote $\mathbf{z}_k^{[1:r_{12}]}$ and $\tilde{\mathbf{z}}_k^{[1:r_{12}]}$ to be the vectors containing two different sets of the first r_{12} canonical variables associated with \mathbf{x}_k . Then, there exists an orthogonal matrix \mathbf{O}_{z_k} such that $\tilde{\mathbf{z}}_k^{[1:r_{12}]} = \mathbf{O}_{z_k} \mathbf{z}_k^{[1:r_{12}]}$. Let $\mathbf{B}_k = \text{cov}(\mathbf{x}_k, \mathbf{z}_k^{[1:r_{12}]})$ and $\tilde{\mathbf{B}}_k = \text{cov}(\mathbf{x}_k, \tilde{\mathbf{z}}_k^{[1:r_{12}]})$. We have $\tilde{\mathbf{B}}_k = \text{cov}(\mathbf{x}_k, \mathbf{z}_k^{[1:r_{12}]}) \mathbf{O}_{z_k}^\top = \mathbf{B}_k \mathbf{O}_{z_k}^\top$. Thus, $\text{colsp}(\tilde{\mathbf{B}}_k) = \text{colsp}(\mathbf{B}_k)$. Define $\tilde{\mathbf{B}}_{2A} = [\tilde{\mathbf{B}}_2; \mathbf{0}_{(p_1-p_2) \times r_{12}}]$. We still have $\text{colsp}(\mathbf{P}\tilde{\mathbf{B}}_{2A}) = \text{colsp}(\mathbf{P}\mathbf{B}_{2A})$. Let $\{\tilde{\mathbf{V}}_{B_k}\}_{k=1}^2$ be the matrices whose columns $\{\tilde{\mathbf{V}}_{B_1}^{[:,\ell]}, \tilde{\mathbf{V}}_{B_2}^{[:,\ell]}\}_{\ell=1}^{r_{12}}$ are another pair of principal vectors of $\text{colsp}(\mathbf{B}_1)$ and $\text{colsp}(\mathbf{P}\mathbf{B}_{2A})$ with $\theta(\tilde{\mathbf{V}}_{B_1}^{[:,\ell]}, \tilde{\mathbf{V}}_{B_2}^{[:,\ell]}) = \theta_{B,\ell}$. There exist orthogonal matrices $\{\mathbf{O}_{V_k}\}_{k=1}^2$ such that $\tilde{\mathbf{V}}_{B_k} = \mathbf{V}_{B_k} \mathbf{O}_{V_k}$. Let $\Lambda_B = \text{diag}(\cos \theta_{B,1}, \dots, \cos \theta_{B,r_{12}})$. Note that $\Lambda_B = \tilde{\mathbf{V}}_{B_1}^\top \tilde{\mathbf{V}}_{B_2} = \mathbf{O}_{V_1}^\top \mathbf{V}_{B_1}^\top \mathbf{V}_{B_2} \mathbf{O}_{V_2} = \mathbf{O}_{V_1}^\top \Lambda_B \mathbf{O}_{V_2}$. Then, $\mathbf{O}_{V_k} = \text{diag}(\mathbf{M}_{k1}, \dots, \mathbf{M}_{km}, \mathbf{M}_{k,m+1})$, where $\mathbf{M}_{k\ell}$, $\ell \leq m$ is an orthogonal matrix with column dimension equal to the repetition number of the ℓ -th largest distinct nonzero singular value of Λ_B , and $\mathbf{M}_{k,m+1}$ might be an empty matrix. By $\mathbf{O}_{V_1} \Lambda_B = \Lambda_B \mathbf{O}_{V_2}$, we obtain $\mathbf{M}_{1\ell} = \mathbf{M}_{2\ell}$ for all $\ell \leq m$. Define $r_\lambda = \text{rank}(\Lambda_B)$,

$$\tilde{\mathbf{c}}_{B,\ell} = \frac{1}{2} \left(1 - \sqrt{\frac{1 - \cos \theta_{B,\ell}}{1 + \cos \theta_{B,\ell}}} \right) \left(\tilde{\mathbf{V}}_{B_1}^{[:,\ell]} + \tilde{\mathbf{V}}_{B_2}^{[:,\ell]} \right),$$

and $\mathbf{A}_B = \text{diag}(a_{B,1}, \dots, a_{B,r_{12}})$ with $a_{B,\ell} = \frac{1}{2} \left[1 - \left(\frac{1 - \cos \theta_{B,\ell}}{1 + \cos \theta_{B,\ell}} \right)^{1/2} \right]$ for $\ell \leq r_{12}$. Note that

$$\begin{aligned}
[\tilde{\mathbf{c}}_{B,\ell}]_{\ell=1}^{r_{12}} \tilde{\mathbf{V}}_{B_k}^\top &= [\tilde{\mathbf{c}}_{B,\ell}]_{\ell=1}^{r_\lambda} (\tilde{\mathbf{V}}_{B_k}^{[:,1:r_\lambda]})^\top \\
&= (\tilde{\mathbf{V}}_{B_1}^{[:,1:r_\lambda]} + \tilde{\mathbf{V}}_{B_2}^{[:,1:r_\lambda]}) \mathbf{A}_B^{[1:r_\lambda,1:r_\lambda]} (\tilde{\mathbf{V}}_{B_k}^{[:,1:r_\lambda]})^\top \\
&= (\mathbf{V}_{B_1}^{[:,1:r_\lambda]} + \mathbf{V}_{B_2}^{[:,1:r_\lambda]}) \text{diag}(\mathbf{M}_{1\ell}, \dots, \mathbf{M}_{1m}) \mathbf{A}_B^{[1:r_\lambda,1:r_\lambda]} \\
&\quad \cdot (\text{diag}(\mathbf{M}_{1\ell}, \dots, \mathbf{M}_{1m}))^\top (\mathbf{V}_{B_k}^{[:,1:r_\lambda]})^\top \\
&= (\mathbf{V}_{B_1}^{[:,1:r_\lambda]} + \mathbf{V}_{B_2}^{[:,1:r_\lambda]}) \mathbf{A}_B^{[1:r_\lambda,1:r_\lambda]} (\mathbf{V}_{B_k}^{[:,1:r_\lambda]})^\top \\
&= [\mathbf{c}_{B,\ell}]_{\ell=1}^{r_\lambda} (\mathbf{V}_{B_k}^{[:,1:r_\lambda]})^\top \\
&= [\mathbf{c}_{B,\ell}]_{\ell=1}^{r_{12}} \mathbf{V}_{B_k}^\top.
\end{aligned}$$

Hence, $[\mathbf{c}_{B,\ell}]_{\ell=1}^{r_{12}} \mathbf{V}_{B_k}^\top$ is unique for $k = 1, 2$. By Theorem 2 in Shu et al. (2019), we have that \mathbf{c}_k is unique for $k = 1, 2$. Thus, both $\mathbf{B}_1([\mathbf{c}_\ell]_{\ell=1}^{r_{12}})^\top$ and $\mathbf{P}\mathbf{B}_{2A}([\mathbf{c}_\ell]_{\ell=1}^{r_{12}})^\top$ are unique. Then by definitions, we obtain the uniqueness of \mathbf{c}_1^* and \mathbf{c}_2^* . Hence, $\mathbf{c} = \frac{1}{2} \sum_{k=1}^2 [\text{tr}(\boldsymbol{\Sigma}_k)]^{-1/2} \mathbf{c}_k^*$ is unique. \square

Proof of Theorem 2. Let $\tilde{r}_k = \text{rank}(\hat{\mathbf{X}}_k)$. From (S.17) in Shu et al. (2019), we have $\tilde{r}_k = r_k$ with probability tending to 1 as $n \rightarrow \infty$. Due to Lemma S.1 in Shu et al. (2019), we simply assume $\tilde{r}_k = r_k$ in the rest of the proof. Thus, $\hat{\boldsymbol{\Lambda}}_k$ is rank- r_k , and then $\hat{\mathbf{B}}_k = \hat{\mathbf{V}}_k \hat{\boldsymbol{\Lambda}}_k^{1/2} \hat{\mathbf{U}}_{\theta_k}^{[:,1:r_{12}]}$ is rank- r_{12} .

From (S.7) of Shu et al. (2019), we have $\lambda_1(\boldsymbol{\Sigma}_k) \asymp \lambda_{r_k}(\boldsymbol{\Sigma}_k)$. By Weyls inequality (see Theorem 3.3.16(c) in Horn and Johnson (1994)) and Assumption 1 (i) and (v), $\kappa_1 \leq \lambda_{k,r_k+1} = |\lambda_{k,r_k+1} - \lambda_{r_k+1}(\boldsymbol{\Sigma}_k)| \leq \lambda_1(\text{cov}(\mathbf{e}_k)) = \|\text{cov}(\mathbf{e}_k)\|_2 \leq \|\text{cov}(\mathbf{e}_k)\|_\infty \leq s_0$. Thus, $\lambda_1(\boldsymbol{\Sigma}_k) \asymp \lambda_{r_k}(\boldsymbol{\Sigma}_k) \asymp R_k$.

Let $\tilde{\mathbf{Q}}_k \in \mathbb{R}^{p_k \times r_{12}}$ be the left singular matrix of \mathbf{B}_k . Note that $\|\mathbf{B}_k\|_2 \leq \|\mathbf{V}_k \boldsymbol{\Lambda}_k^{1/2}\|_2 \|\mathbf{U}_{\theta_k}^{[:,1:r_{12}]}\|_2 = \lambda_1^{1/2}(\boldsymbol{\Sigma}_k)$. By (S.31) in Shu et al. (2019), we have

$$\|\hat{\mathbf{B}}_k - \mathbf{B}_k\|_2 = O_P(\lambda_1^{1/2}(\boldsymbol{\Sigma}_k) \delta_\theta). \quad (\text{S.1})$$

Thus, $\|\hat{\mathbf{B}}_k\|_2 \leq \|\hat{\mathbf{B}}_k - \mathbf{B}_k\|_2 + \|\mathbf{B}_k\|_2 = O_P(\lambda_1^{1/2}(\boldsymbol{\Sigma}_k))$. By Lemma 1 of Lam and Fan (2009) and then Theorem 3 of Yu et al. (2015), there exists an orthogonal matrix \mathbf{O}_k such that

$$\|\hat{\mathbf{Q}}_k - \tilde{\mathbf{Q}}_k \mathbf{O}_k\|_F \leq \|\hat{\mathbf{Q}}_k \mathbf{O}_k^\top - \tilde{\mathbf{Q}}_k\|_F \|\mathbf{O}_k\|_2 \lesssim_P \lambda_1^{1/2}(\boldsymbol{\Sigma}_k) \|\hat{\mathbf{B}}_k - \mathbf{B}_k\|_2 / \lambda_1(\boldsymbol{\Sigma}_k) \lesssim_P \delta_\theta. \quad (\text{S.2})$$

Here and in the following text, we write $A \lesssim_P B$ if and only if $A = O_P(B)$. Note that for any

real matrices \mathbf{M}_1 and \mathbf{M}_2 , we have

$$\|\widehat{\mathbf{M}}_1\widehat{\mathbf{M}}_2 - \mathbf{M}_1\mathbf{M}_2\|_2 \leq \begin{cases} \|\widehat{\mathbf{M}}_1\|_2\|\widehat{\mathbf{M}}_2 - \mathbf{M}_2\|_2 + \|\mathbf{M}_2\|_2\|\widehat{\mathbf{M}}_1 - \mathbf{M}_1\|_2, \\ \|\mathbf{M}_1\|_2\|\widehat{\mathbf{M}}_2 - \mathbf{M}_2\|_2 + \|\widehat{\mathbf{M}}_2\|_2\|\widehat{\mathbf{M}}_1 - \mathbf{M}_1\|_2, \end{cases} \quad (\text{S.3})$$

and

$$\|\widehat{\mathbf{M}}_1\widehat{\mathbf{M}}_2 - \mathbf{M}_1\mathbf{M}_2\|_F \leq \begin{cases} \|\widehat{\mathbf{M}}_1\|_2\|\widehat{\mathbf{M}}_2 - \mathbf{M}_2\|_F + \|\mathbf{M}_2\|_2\|\widehat{\mathbf{M}}_1 - \mathbf{M}_1\|_F, \\ \|\mathbf{M}_1\|_2\|\widehat{\mathbf{M}}_2 - \mathbf{M}_2\|_F + \|\widehat{\mathbf{M}}_2\|_2\|\widehat{\mathbf{M}}_1 - \mathbf{M}_1\|_F. \end{cases} \quad (\text{S.4})$$

Let $\mathbf{Q}_k = \widetilde{\mathbf{Q}}_k\mathbf{O}_k$ and $\mathbf{Q}_{2A} = [\mathbf{Q}_2; \mathbf{0}_{(p_1-p_2) \times r_{12}}]$. Note that the columns of \mathbf{Q}_k form an orthonormal basis of $\text{colsp}(\mathbf{B}_k)$, and those of $\mathbf{P}\mathbf{Q}_{2A}$ also form an orthonormal basis of $\text{colsp}(\mathbf{P}\mathbf{B}_{2A})$. Let $\Theta_B = \mathbf{Q}_1^\top \mathbf{P}\mathbf{Q}_{2A}$. Then by (S.4) and (S.2), we have

$$\begin{aligned} \|\widehat{\Theta}_B - \Theta_B\|_F &\leq \|\widehat{\mathbf{Q}}_1^\top\|_2\|\mathbf{P}\widehat{\mathbf{Q}}_{2A} - \mathbf{P}\mathbf{Q}_{2A}\|_F + \|\mathbf{P}\mathbf{Q}_{2A}\|_2\|\widehat{\mathbf{Q}}_1^\top - \mathbf{Q}_1^\top\|_F \\ &\leq \|\widehat{\mathbf{Q}}_1^\top\|_2\|\mathbf{P}\|_2\|\widehat{\mathbf{Q}}_{2A} - \mathbf{Q}_{2A}\|_F + \|\mathbf{P}\|_2\|\mathbf{Q}_{2A}\|_2\|\widehat{\mathbf{Q}}_1^\top - \mathbf{Q}_1^\top\|_F \\ &= \|\widehat{\mathbf{Q}}_2 - \mathbf{Q}_2\|_F + \|\widehat{\mathbf{Q}}_1 - \mathbf{Q}_1\|_F \\ &\lesssim_P \delta_\theta, \end{aligned}$$

and

$$\begin{aligned} &\max\{\|\widehat{\Theta}_B\widehat{\Theta}_B^\top - \Theta_B\Theta_B^\top\|_F, \|\widehat{\Theta}_B^\top\widehat{\Theta}_B - \Theta_B^\top\Theta_B\|_F\} \\ &\leq (\|\widehat{\Theta}_B\|_2 + \|\Theta_B\|_2)\|\widehat{\Theta}_B - \Theta_B\|_F \leq 2\|\widehat{\Theta}_B - \Theta_B\|_F \lesssim_P \delta_\theta. \end{aligned}$$

By Weyl's inequality (see Theorem 3.3.16(c) in Horn and Johnson (1994)),

$$\max_{1 \leq \ell \leq r_{12}} |\sigma_\ell(\widehat{\Theta}_B) - \sigma_\ell(\Theta_B)| \leq \|\widehat{\Theta}_B - \Theta_B\|_2 \leq \|\widehat{\Theta}_B - \Theta_B\|_F \lesssim_P \delta_\theta. \quad (\text{S.5})$$

Denote $\{\widetilde{\mathbf{U}}_{B_k}\}_{k=1}^2$ to be one pair of orthogonal matrices such that $\Theta_B = \widetilde{\mathbf{U}}_{B_1}\Lambda_B\widetilde{\mathbf{U}}_{B_2}^\top$. Let $\sigma_{B,1} > \cdots > \sigma_{B,r_B}$ be the distinct singular values of Θ_B , and define $\sigma_{B,r_{12}+1}^2 = -\infty$. By Lemma 1 of Lam and Fan (2009) and then Theorem 2 of Yu et al. (2015), there exists a matrix $\mathbf{O}_{B_k} = \text{diag}(\mathbf{O}_{B_k,1}, \dots, \mathbf{O}_{B_k,r_B})$, where $\mathbf{O}_{B_k,\ell}$ is an orthogonal matrix with column dimension

equal to the repetition number of $\sigma_{B,\ell}$, such that

$$\begin{aligned} \|\widehat{\mathbf{U}}_{B_k} - \widetilde{\mathbf{U}}_{B_k} \mathbf{O}_{B_k}\|_F &\leq \|\widehat{\mathbf{U}}_{B_k} \mathbf{O}_{B_k}^\top - \widetilde{\mathbf{U}}_{B_k}\|_F \|\mathbf{O}_{B_k}\|_2 \\ &\lesssim_P \min \left\{ \delta_\theta / \min_{1 \leq \ell \leq r_B} \{\sigma_{B,\ell}^2 - \sigma_{B,\ell+1}^2\}, 1 \right\} \lesssim_P \delta_\theta. \end{aligned} \quad (\text{S.6})$$

Define $\widetilde{\mathbf{O}}_{B_2} = \text{diag}(\mathbf{O}_{B_1,1}, \dots, \mathbf{O}_{B_1,r_B-1}, \mathbf{O}_{B_1,r_B})$ if $\sigma_{B,r_B} \neq 0$, and otherwise let $\widetilde{\mathbf{O}}_{B_2} = \text{diag}(\mathbf{O}_{B_1,1}, \dots, \mathbf{O}_{B_1,r_B-1}, \mathbf{O}_{B_2,r_B})$. Let $\mathbf{U}_{B_1} = \widetilde{\mathbf{U}}_{B_1} \mathbf{O}_{B_1}$ and $\mathbf{U}_{B_2} = \widetilde{\mathbf{U}}_{B_2} \widetilde{\mathbf{O}}_{B_2}$. We have $\mathbf{U}_{B_1} \mathbf{\Lambda}_B \mathbf{U}_{B_2} = \widetilde{\mathbf{U}}_{B_1} \mathbf{O}_{B_1} \mathbf{\Lambda}_B \widetilde{\mathbf{O}}_{B_2}^\top \widetilde{\mathbf{U}}_{B_2}^\top = \widetilde{\mathbf{U}}_{B_1} \mathbf{\Lambda}_B \widetilde{\mathbf{U}}_{B_2}^\top = \mathbf{\Theta}_B$. Define $\mathbf{U}_{B_2}^* = \widetilde{\mathbf{U}}_{B_2} \mathbf{O}_{B_2}$ and $r_{\theta_B} = \text{rank}(\mathbf{\Theta}_B)$. Then,

$$\mathbf{U}_{B_2}^{[:,(r_{\theta_B}+1):r_{12}]} = \mathbf{U}_{B_2}^{*[:,(r_{\theta_B}+1):r_{12}]} \quad \text{if } r_{\theta_B} < r_{12}, \quad (\text{S.7})$$

$$\|\widehat{\mathbf{U}}_{B_1} - \mathbf{U}_{B_1}\|_F \lesssim_P \delta_\theta, \quad (\text{S.8})$$

and

$$\|\widehat{\mathbf{U}}_{B_2} - \mathbf{U}_{B_2}^*\|_F \lesssim_P \delta_\theta. \quad (\text{S.9})$$

By (S.3), (S.5) and the above two inequalities,

$$\begin{aligned} &\left\| \widehat{\mathbf{U}}_{B_1} \widehat{\mathbf{\Lambda}}_B \widehat{\mathbf{U}}_{B_2}^\top - \mathbf{U}_{B_1} \mathbf{\Lambda}_B \mathbf{U}_{B_2}^{*\top} \right\|_2 \\ &\leq \|\widehat{\mathbf{U}}_{B_1} \widehat{\mathbf{\Lambda}}_B - \mathbf{U}_{B_1} \mathbf{\Lambda}_B\|_2 \|\widehat{\mathbf{U}}_{B_2}^\top\|_2 + \|\mathbf{U}_{B_1} \mathbf{\Lambda}_B\|_2 \|\widehat{\mathbf{U}}_{B_2}^\top - \mathbf{U}_{B_2}^{*\top}\|_2 \\ &\leq \|\widehat{\mathbf{U}}_{B_1} - \mathbf{U}_{B_1}\|_2 \|\mathbf{\Lambda}_B\|_2 + \|\widehat{\mathbf{U}}_{B_1}\|_2 \|\widehat{\mathbf{\Lambda}}_B - \mathbf{\Lambda}_B\|_2 + \|\mathbf{\Lambda}_B\|_2 \|\widehat{\mathbf{U}}_{B_2}^\top - \mathbf{U}_{B_2}^{*\top}\|_2 \\ &\lesssim_P \delta_\theta. \end{aligned}$$

By the above inequality, $\|\widehat{\mathbf{\Theta}}_B - \mathbf{\Theta}_B\|_2 \lesssim_P \delta_\theta$, and the triangular inequality of matrix norms, we have

$$\|\mathbf{U}_{B_1} \mathbf{\Lambda}_B (\mathbf{U}_{B_2} - \mathbf{U}_{B_2}^*)^\top\|_2 \lesssim_P \delta_\theta.$$

It follows that

$$\begin{aligned} &\|\mathbf{U}_{B_2}^{[:,1:r_{\theta_B}]} - \mathbf{U}_{B_2}^{*[:,1:r_{\theta_B}]}\|_F \\ &\leq \sqrt{r_{12}} \|\mathbf{U}_{B_2}^{[:,1:r_{\theta_B}]} - \mathbf{U}_{B_2}^{*[:,1:r_{\theta_B}]}\|_2 \\ &\leq \sqrt{r_{12}} \left\| \mathbf{\Lambda}_B^\dagger \right\|_2 \|\mathbf{U}_{B_1}^\top\|_2 \|\mathbf{U}_{B_1} \mathbf{\Lambda}_B (\mathbf{U}_{B_2} - \mathbf{U}_{B_2}^*)^\top\|_2 \\ &\lesssim_P \delta_\theta. \end{aligned} \quad (\text{S.10})$$

Combining (S.10), (S.7) and (S.9) yields

$$\|\widehat{\mathbf{U}}_{B_2} - \mathbf{U}_{B_2}\|_F \lesssim_P \delta_\theta. \quad (\text{S.11})$$

By (7), we have that the ℓ -th columns of $\mathbf{V}_{B_1} := \mathbf{Q}_1 \mathbf{U}_{B_1}$ and $\mathbf{V}_{B_2} := \mathbf{P} \mathbf{Q}_{2A} \mathbf{U}_{B_2}$ are the ℓ -th pair of principal vectors of $\text{colsp}(\mathbf{B}_1)$ and $\text{colsp}(\mathbf{P} \mathbf{B}_{2A})$. By (S.4), (S.2) and (S.8), we have

$$\begin{aligned} \|\widehat{\mathbf{V}}_{B_1} - \mathbf{V}_{B_1}\|_F &= \|\mathbf{Q}_1 \mathbf{U}_{B_1} - \widehat{\mathbf{Q}}_1 \widehat{\mathbf{U}}_{B_1}\|_2 \\ &\leq \|\widehat{\mathbf{U}}_{B_1}\|_2 \|\widehat{\mathbf{Q}}_1 - \mathbf{Q}_1\|_F + \|\mathbf{Q}_1\|_2 \|\widehat{\mathbf{U}}_{B_1} - \mathbf{U}_{B_1}\|_F \\ &\lesssim_P \delta_\theta. \end{aligned} \quad (\text{S.12})$$

Similarly, by (S.11) we obtain

$$\|\widehat{\mathbf{V}}_{B_2} - \mathbf{V}_{B_2}\|_F \lesssim_P \delta_\theta. \quad (\text{S.13})$$

Then, together with (S.4) and (S.1), we have

$$\|\widehat{\mathbf{V}}_{B_1}^\top \widehat{\mathbf{B}}_1 - \mathbf{V}_{B_1}^\top \mathbf{B}_1\|_F \leq \|\widehat{\mathbf{B}}_1\|_2 \|\widehat{\mathbf{V}}_{B_1}^\top - \mathbf{V}_{B_1}^\top\|_F + \|\mathbf{V}_{B_1}^\top\|_2 \|\widehat{\mathbf{B}}_1 - \mathbf{B}_1\|_F \lesssim_P \lambda_1^{1/2}(\boldsymbol{\Sigma}_1) \delta_\theta, \quad (\text{S.14})$$

and similarly,

$$\|\widehat{\mathbf{V}}_{B_2}^\top \widehat{\mathbf{P}} \mathbf{B}_{2A} - \mathbf{V}_{B_2}^\top \mathbf{P} \mathbf{B}_{2A}\|_F \lesssim_P \lambda_1^{1/2}(\boldsymbol{\Sigma}_2) \delta_\theta. \quad (\text{S.15})$$

By the results given in (S.16), (S.17) and (S.7) of Shu et al. (2019), we have $|\lambda_\ell(\widehat{\boldsymbol{\Sigma}}_k) - \lambda_\ell(\boldsymbol{\Sigma}_k)| \lesssim_P \lambda_1(\boldsymbol{\Sigma}_k)/\sqrt{n}$ for all $\ell \leq r_k$, $[\text{tr}(\widehat{\boldsymbol{\Sigma}}_k)]^{1/2} = [\sum_{\ell=1}^{r_k} \lambda_\ell(\widehat{\boldsymbol{\Sigma}}_k)]^{1/2} \geq [r_k(1 - o_P(1))\lambda_{r_k}(\boldsymbol{\Sigma}_k)]^{1/2}$, and $\lambda_1(\boldsymbol{\Sigma}_k) \asymp \lambda_{r_k}(\boldsymbol{\Sigma}_k)$. Then by the mean value theorem, we obtain

$$\begin{aligned} |[\text{tr}(\widehat{\boldsymbol{\Sigma}}_k)]^{1/2} - [\text{tr}(\boldsymbol{\Sigma}_k)]^{1/2}| &\leq \frac{1}{2} |\text{tr}(\widehat{\boldsymbol{\Sigma}}_k) - \text{tr}(\boldsymbol{\Sigma}_k)| \cdot \max\{[\text{tr}(\widehat{\boldsymbol{\Sigma}}_k)]^{-1/2}, [\text{tr}(\boldsymbol{\Sigma}_k)]^{-1/2}\} \\ &\lesssim_P \lambda_1^{1/2}(\boldsymbol{\Sigma}_k)/\sqrt{n}. \end{aligned} \quad (\text{S.16})$$

Hence,

$$\begin{aligned} |[\text{tr}(\widehat{\boldsymbol{\Sigma}}_k)]^{-1/2} - [\text{tr}(\boldsymbol{\Sigma}_k)]^{-1/2}| &= |[\text{tr}(\widehat{\boldsymbol{\Sigma}}_k)]^{1/2} - [\text{tr}(\boldsymbol{\Sigma}_k)]^{1/2}| / ([\text{tr}(\widehat{\boldsymbol{\Sigma}}_k)]^{1/2} [\text{tr}(\boldsymbol{\Sigma}_k)]^{1/2}) \\ &\lesssim_P \lambda_1^{-1/2}(\boldsymbol{\Sigma}_k)/\sqrt{n}. \end{aligned} \quad (\text{S.17})$$

By (S.4), (S.14) and (S.17),

$$\begin{aligned} & \left\| \widehat{\mathbf{V}}_{B_1}^\top \widehat{\mathbf{B}}_1 [\text{tr}(\widehat{\boldsymbol{\Sigma}}_1)]^{-1/2} - \mathbf{V}_{B_1}^\top \mathbf{B}_1 [\text{tr}(\boldsymbol{\Sigma}_1)]^{-1/2} \right\|_F \\ & \lesssim_P \lambda_1^{-1/2}(\boldsymbol{\Sigma}_1) (\lambda_1^{1/2}(\boldsymbol{\Sigma}_1) \delta_\theta) + \lambda_1^{1/2}(\boldsymbol{\Sigma}_1) \lambda_1^{-1/2}(\boldsymbol{\Sigma}_1) / \sqrt{n} \\ & \lesssim_P \delta_\theta. \end{aligned}$$

Similarly, by (S.15), $\left\| \widehat{\mathbf{V}}_{B_2}^\top \widehat{\mathbf{P}} \widehat{\mathbf{B}}_{2A} [\text{tr}(\widehat{\boldsymbol{\Sigma}}_2)]^{-1/2} - \mathbf{V}_{B_2}^\top \mathbf{P} \mathbf{B}_{2A} [\text{tr}(\boldsymbol{\Sigma}_2)]^{-1/2} \right\|_F \lesssim_P \delta_\theta$. Thus,

$$\begin{aligned} & \left\| (\widehat{\mathbf{V}}_{B_1}^\top \widehat{\mathbf{B}}_1 [\text{tr}(\widehat{\boldsymbol{\Sigma}}_1)]^{-1/2} + \widehat{\mathbf{V}}_{B_2}^\top \widehat{\mathbf{P}} \widehat{\mathbf{B}}_{2A} [\text{tr}(\widehat{\boldsymbol{\Sigma}}_2)]^{-1/2}) \right. \\ & \quad \left. - (\mathbf{V}_{B_1}^\top \mathbf{B}_1 [\text{tr}(\boldsymbol{\Sigma}_1)]^{-1/2} + \mathbf{V}_{B_2}^\top \mathbf{P} \mathbf{B}_{2A} [\text{tr}(\boldsymbol{\Sigma}_2)]^{-1/2}) \right\|_F \lesssim_P \delta_\theta. \end{aligned} \quad (\text{S.18})$$

Define $\mathbf{C}_B = [\mathbf{c}_{B,\ell}]_{\ell=1}^{r_{12}}$ and $\mathbf{A}_B = \text{diag}(a_{B,1}, \dots, a_{B,r_{12}})$ with $a_{B,\ell} = \frac{1}{2} \left[1 - \left(\frac{1 - \Lambda_B^{[\ell,\ell]}}{1 + \Lambda_B^{[\ell,\ell]}} \right)^{1/2} \right]$. We have $\mathbf{C}_B = (\mathbf{V}_{B_1} + \mathbf{V}_{B_2}) \mathbf{A}_B$. By the same technique used to derive (S.32) in Shu et al. (2019), we have $\|\widehat{\mathbf{A}}_B - \mathbf{A}_B\|_F \lesssim_P \delta_\theta^{1/2}$. From (S.12) and (S.13), $\|(\widehat{\mathbf{V}}_{B_1} + \widehat{\mathbf{V}}_{B_2}) - (\mathbf{V}_{B_1} + \mathbf{V}_{B_2})\|_F \lesssim_P \delta_\theta$. Then by (S.4),

$$\|\widehat{\mathbf{C}}_B - \mathbf{C}_B\|_F \lesssim_P \delta_\theta^{1/2} + \delta_\theta \lesssim_P \delta_\theta^{1/2}. \quad (\text{S.19})$$

From (S.23) in Shu et al. (2019), $\|\widehat{\boldsymbol{\Theta}} - \boldsymbol{\Theta}\|_F \lesssim \delta_\theta$. Using the same proof technique for (S.8) and (S.11), we have $\|\widehat{\mathbf{U}}_{\theta k}^{[:,1:r_{12}]} - \mathbf{U}_{\theta k}^{[:,1:r_{12}]}\|_F \lesssim_P \delta_\theta$. Then following the same proof lines for (S.28) in Shu et al. (2019), we can obtain

$$\left\| (\widehat{\mathbf{U}}_{\theta k}^{[:,1:r_{12}]})^\top \widehat{\boldsymbol{\Lambda}}_k^{-1/2} \widehat{\mathbf{V}}_k^\top - (\mathbf{U}_{\theta k}^{[:,1:r_{12}]})^\top \boldsymbol{\Lambda}_k^{-1/2} \mathbf{V}_k^\top \right\|_F \lesssim_P \lambda_1^{-1/2}(\boldsymbol{\Sigma}_k) \delta_\theta.$$

From the results given in (S.9), (S.13), (S.15) and (S.32) of Shu et al. (2019), we have that $\max\{\|\widehat{\mathbf{X}}_k\|_F, \|\mathbf{X}_k\|_F\} \lesssim_P \sqrt{n \lambda_1(\boldsymbol{\Sigma}_k)}$, $\|\widehat{\mathbf{X}}_k - \mathbf{X}_k\|_F \lesssim_P \min\{\sqrt{\lambda_1(\boldsymbol{\Sigma}_k)/n} + \sqrt{p_k \log p_k}, \sqrt{n \lambda_1(\boldsymbol{\Sigma}_k)}\}$, and $\|\widehat{\mathbf{A}}_C - \mathbf{A}_C\|_F \lesssim_P \delta_\theta^{1/2}$, where $\mathbf{A}_C = \text{diag}(a_1, \dots, a_{r_{12}})$ with $a_\ell = \frac{1}{2} \left[1 - \left(\frac{1 - \sigma_\ell(\boldsymbol{\Theta})}{1 + \sigma_\ell(\boldsymbol{\Theta})} \right)^{1/2} \right]$. Let $\mathbf{Z}_k = \mathbf{U}_{\theta k}^\top \boldsymbol{\Lambda}_k^{-1/2} \mathbf{V}_k^\top \mathbf{X}_k$ and $\mathbf{C}_0 = \mathbf{A}_C \sum_{j=1}^2 \mathbf{Z}_j^{[1:r_{12},:]}$, which are the sample matrices of \mathbf{z}_k and

$(c_1, \dots, c_{r_{12}})^\top$, respectively. Then by (S.4),

$$\begin{aligned}
& \left\| \widehat{\mathbf{Z}}_k^{[1:r_{12},:]} - \mathbf{Z}_k^{[1:r_{12},:]} \right\|_F \\
&= \left\| \left(\widehat{\mathbf{U}}_{\theta k}^{[:,1:r_{12}]} \right)^\top \widehat{\mathbf{\Lambda}}_k^{-1/2} \widehat{\mathbf{V}}_k^\top \widehat{\mathbf{X}}_k - \left(\mathbf{U}_{\theta k}^{[:,1:r_{12}]} \right)^\top \mathbf{\Lambda}_k^{-1/2} \mathbf{V}_k^\top \mathbf{X}_k \right\|_F \\
&\lesssim_P \lambda_1^{-1/2}(\mathbf{\Sigma}_k) \delta_\theta \sqrt{n \lambda_1(\mathbf{\Sigma}_k)} + \min\{ \sqrt{\lambda_1(\mathbf{\Sigma}_k)/n} + \sqrt{p_k \log p_k}, \sqrt{n \lambda_1(\mathbf{\Sigma}_k)} \} / \sqrt{\lambda_1(\mathbf{\Sigma}_k)} \\
&\lesssim_P \delta_\theta \sqrt{n},
\end{aligned}$$

and thus,

$$\|\widehat{\mathbf{C}}_0 - \mathbf{C}_0\|_F \lesssim_P \delta_\theta^{1/2} \sqrt{n}. \quad (\text{S.20})$$

From (S.18), (S.19), (S.20) and (S.4), we obtain

$$\|\widehat{\mathbf{C}} - \mathbf{C}\|_2 \leq \|\widehat{\mathbf{C}} - \mathbf{C}\|_F = O_P(\delta_\theta^{1/2} \sqrt{n}). \quad (\text{S.21})$$

Combining (S.16) and (S.21) yields

$$\|\widehat{\mathbf{C}}^{(k)} - \mathbf{C}^{(k)}\|_2 \leq \|\widehat{\mathbf{C}}^{(k)} - \mathbf{C}^{(k)}\|_F \lesssim_P \delta_\theta^{1/2} \sqrt{n} \cdot \lambda_1^{1/2}(\mathbf{\Sigma}_k).$$

By (S.14) in Shu et al. (2019), there exists a constant $\kappa_3 \in (0, 1]$ such that $\|\mathbf{X}_k\|_F \geq \|\mathbf{X}_k\|_2 \geq [\kappa_3 + o_P(1)] \sqrt{n \lambda_1(\mathbf{\Sigma}_k)}$. Hence,

$$\frac{\|\widehat{\mathbf{C}} - \mathbf{C}\|_\star^2}{\frac{1}{2}(\|\mathbf{X}_1^S\|_\star^2 + \|\mathbf{X}_2^S\|_\star^2)} = O_P(\delta_\theta),$$

and

$$\frac{\|\widehat{\mathbf{C}}^{(k)} - \mathbf{C}^{(k)}\|_\star^2}{\|\mathbf{X}_k\|_\star^2} = O_P(\delta_\theta).$$

Let $\mathbf{c}_0 = (c_1, \dots, c_{r_{12}})^\top$ and $\mathbf{z}_c = [\mathbf{z}_1^{[1:r_{12}]}; \mathbf{z}_2^{[1:r_{12}]}]$. Define $\mathbf{Z}_c = [\mathbf{Z}_1^{[1:r_{12},:]}; \mathbf{Z}_2^{[1:r_{12},:]}]$, which is the sample matrix of \mathbf{z}_c . We have $\mathbf{c}_0 = \mathbf{A}_C[\mathbf{I}_{r_{12} \times r_{12}}, \mathbf{I}_{r_{12} \times r_{12}}] \mathbf{z}_c$ and $\mathbf{C}_0 = \mathbf{A}_C[\mathbf{I}_{r_{12} \times r_{12}}, \mathbf{I}_{r_{12} \times r_{12}}] \mathbf{Z}_c$.

From the central limit theorem,

$$\left\| \frac{1}{n} \mathbf{Z}_c \mathbf{Z}_c^\top - \text{cov}(\mathbf{z}_c) \right\|_F \leq 2r_{12} \left\| \frac{1}{n} \mathbf{Z}_c \mathbf{Z}_c^\top - \text{cov}(\mathbf{z}_c) \right\|_{\max} \lesssim_P n^{-1/2}.$$

Hence,

$$\left\| \frac{1}{n} \mathbf{C}_0 \mathbf{C}_0^\top - \text{cov}(\mathbf{c}_0) \right\|_F \leq \left\| \frac{1}{n} \mathbf{Z}_c \mathbf{Z}_c^\top - \text{cov}(\mathbf{z}_c) \right\|_F \left\| \mathbf{A}_C[\mathbf{I}_{r_{12} \times r_{12}}, \mathbf{I}_{r_{12} \times r_{12}}] \right\|_F^2 \lesssim_P n^{-1/2}.$$

Then,

$$\left\| \frac{1}{n} \mathbf{C} \mathbf{C}^\top - \text{cov}(\mathbf{c}) \right\|_F \leq \left\| \frac{1}{n} \mathbf{C}_0 \mathbf{C}_0^\top - \text{cov}(\mathbf{c}_0) \right\|_F \|\mathbf{C}_B \mathbf{S}\|_F^2 \lesssim_P n^{-1/2}.$$

By (S.21), we have

$$\left\| \frac{1}{n} \widehat{\mathbf{C}} \widehat{\mathbf{C}}^\top - \frac{1}{n} \mathbf{C} \mathbf{C}^\top \right\|_F \leq \frac{1}{n} \|\widehat{\mathbf{C}} - \mathbf{C}\|_F (\|\widehat{\mathbf{C}}\|_F + \|\mathbf{C}\|_F) \lesssim_P \delta_\theta^{1/2}.$$

Combining the above two inequalities yields

$$\left\| \frac{1}{n} \widehat{\mathbf{C}} \widehat{\mathbf{C}}^\top - \text{cov}(\mathbf{c}) \right\|_F \lesssim_P \delta_\theta^{1/2}.$$

By Weyl's inequality (see Theorem 3.3.16(c) in Horn and Johnson (1994)),

$$\max_{\ell \leq r_{12}} \left| \lambda_\ell \left(\frac{1}{n} \widehat{\mathbf{C}} \widehat{\mathbf{C}}^\top \right) - \lambda_\ell (\text{cov}(\mathbf{c})) \right| \leq \left\| \frac{1}{n} \widehat{\mathbf{C}} \widehat{\mathbf{C}}^\top - \text{cov}(\mathbf{c}) \right\|_2 \leq \left\| \frac{1}{n} \widehat{\mathbf{C}} \widehat{\mathbf{C}}^\top - \text{cov}(\mathbf{c}) \right\|_F \lesssim_P \delta_\theta^{1/2}.$$

Then,

$$\left| \text{tr} \left(\frac{1}{n} \widehat{\mathbf{C}} \widehat{\mathbf{C}}^\top \right) - \text{tr}(\text{cov}(\mathbf{c})) \right| \leq \sum_{\ell=1}^{r_{12}} \left| \lambda_\ell \left(\frac{1}{n} \widehat{\mathbf{C}} \widehat{\mathbf{C}}^\top \right) - \lambda_\ell (\text{cov}(\mathbf{c})) \right| \lesssim_P \delta_\theta^{1/2}.$$

The proof is complete. \square

Proof of Theorem 3. By (S.2), there exists a matrix \mathbf{Q}_k , whose columns form an orthonormal basis of $\text{colsp}(\mathbf{B}_k)$, such that $\|\widehat{\mathbf{Q}}_k - \mathbf{Q}_k\|_F = O_P(\delta_\theta)$. Note that $\text{tr}(\mathbf{Q}_1^\top \mathbf{P} \mathbf{Q}_{2A} (\mathbf{Q}_1^\top \mathbf{P} \mathbf{Q}_{2A})^\top) = \|\mathbf{Q}_1^\top \mathbf{P} \mathbf{Q}_{2A}\|_F^2$. Then by (S.4), for any $\mathbf{P} \in \Pi_{p_1}$, we have

$$\begin{aligned} & \left| \|\mathbf{Q}_1^\top \mathbf{P} \mathbf{Q}_{2A}\|_F^2 - \|\widehat{\mathbf{Q}}_1^\top \mathbf{P} \widehat{\mathbf{Q}}_{2A}\|_F^2 \right| \\ & \leq \left| \|\mathbf{Q}_1^\top \mathbf{P} \mathbf{Q}_{2A}\|_F - \|\widehat{\mathbf{Q}}_1^\top \mathbf{P} \widehat{\mathbf{Q}}_{2A}\|_F \right| (\|\mathbf{Q}_1^\top \mathbf{P} \mathbf{Q}_{2A}\|_F + \|\widehat{\mathbf{Q}}_1^\top \mathbf{P} \widehat{\mathbf{Q}}_{2A}\|_F) \\ & \leq \|\mathbf{Q}_1^\top \mathbf{P} \mathbf{Q}_{2A} - \widehat{\mathbf{Q}}_1^\top \mathbf{P} \widehat{\mathbf{Q}}_{2A}\|_F (\|\mathbf{Q}_1^\top \mathbf{P}\|_F \|\mathbf{Q}_{2A}\|_F + \|\widehat{\mathbf{Q}}_1^\top \mathbf{P}\|_F \|\widehat{\mathbf{Q}}_{2A}\|_F) \\ & \leq (\|\widehat{\mathbf{Q}}_1^\top\|_2 \|\mathbf{P} \mathbf{Q}_{2A} - \widehat{\mathbf{P}} \widehat{\mathbf{Q}}_{2A}\|_F + \|\mathbf{P} \mathbf{Q}_{2A}\|_2 \|\mathbf{Q}_1^\top - \widehat{\mathbf{Q}}_1^\top\|_F) 2r_k \\ & = O_P(\delta_\theta). \end{aligned}$$

Hence, $\left| \|\mathbf{Q}_1^\top \mathbf{P} \mathbf{Q}_{2A}\|_F^2 - \|\widehat{\mathbf{Q}}_1^\top \widehat{\mathbf{P}} \widehat{\mathbf{Q}}_{2A}\|_F^2 \right| = O_P(\delta_\theta) = \left| \|\mathbf{Q}_1^\top \widehat{\mathbf{P}} \mathbf{Q}_{2A}\|_F^2 - \|\widehat{\mathbf{Q}}_1^\top \widehat{\mathbf{P}} \widehat{\mathbf{Q}}_{2A}\|_F^2 \right|$. Note

that $\|\mathbf{Q}_1^\top \widehat{\mathbf{P}}_* \mathbf{Q}_{2A}\|_F^2 \leq \|\mathbf{Q}_1^\top \mathbf{P}_* \mathbf{Q}_{2A}\|_F^2$ and $\|\widehat{\mathbf{Q}}_1^\top \mathbf{P}_* \widehat{\mathbf{Q}}_{2A}\|_F^2 \leq \|\widehat{\mathbf{Q}}_1^\top \widehat{\mathbf{P}}_* \widehat{\mathbf{Q}}_{2A}\|_F^2$. We have

$$\begin{aligned}
0 &\leq \|\mathbf{Q}_1^\top \mathbf{P}_* \mathbf{Q}_{2A}\|_F^2 - \|\mathbf{Q}_1^\top \widehat{\mathbf{P}}_* \mathbf{Q}_{2A}\|_F^2 \\
&= (\|\mathbf{Q}_1^\top \mathbf{P}_* \mathbf{Q}_{2A}\|_F^2 - \|\widehat{\mathbf{Q}}_1^\top \mathbf{P}_* \widehat{\mathbf{Q}}_{2A}\|_F^2) + (\|\widehat{\mathbf{Q}}_1^\top \widehat{\mathbf{P}}_* \widehat{\mathbf{Q}}_{2A}\|_F^2 - \|\mathbf{Q}_1^\top \widehat{\mathbf{P}}_* \mathbf{Q}_{2A}\|_F^2) \\
&\quad + (\|\widehat{\mathbf{Q}}_1^\top \mathbf{P}_* \widehat{\mathbf{Q}}_{2A}\|_F^2 - \|\widehat{\mathbf{Q}}_1^\top \widehat{\mathbf{P}}_* \widehat{\mathbf{Q}}_{2A}\|_F^2) \\
&\leq \left| \|\mathbf{Q}_1^\top \mathbf{P}_* \mathbf{Q}_{2A}\|_F^2 - \|\widehat{\mathbf{Q}}_1^\top \mathbf{P}_* \widehat{\mathbf{Q}}_{2A}\|_F^2 \right| + \left| \|\widehat{\mathbf{Q}}_1^\top \widehat{\mathbf{P}}_* \widehat{\mathbf{Q}}_{2A}\|_F^2 - \|\mathbf{Q}_1^\top \widehat{\mathbf{P}}_* \mathbf{Q}_{2A}\|_F^2 \right| \\
&= O_P(\delta_\theta).
\end{aligned}$$

Hence, $\left| \text{tr}(\mathbf{Q}_1^\top \widehat{\mathbf{P}}_* \mathbf{Q}_{2A} (\mathbf{Q}_1^\top \widehat{\mathbf{P}}_* \mathbf{Q}_{2A})^\top) - \text{tr}(\mathbf{Q}_1^\top \mathbf{P}_* \mathbf{Q}_{2A} (\mathbf{Q}_1^\top \mathbf{P}_* \mathbf{Q}_{2A})^\top) \right| = O_P(\delta_\theta)$. \square

S.2 Additional Simulation Results

Figures S.1–S.14 display the simulation results for the CDPA estimators under Setups 1 and 2. The result analysis given in Section 4 generally holds here.

References

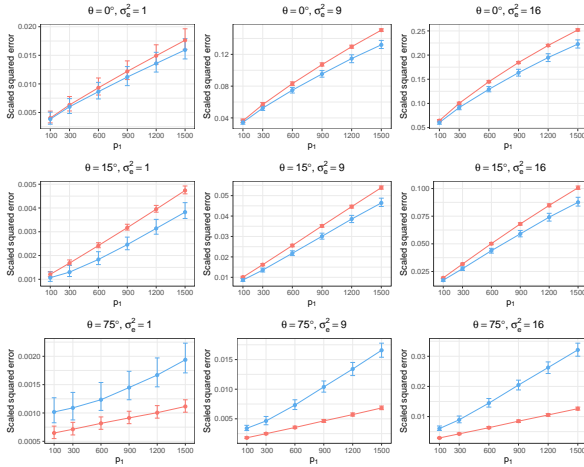
- Barch, D. M., Burgess, G. C., Harms, M. P., Petersen, S. E., Schlaggar, B. L., Corbetta, M., Glasser, M. F., Curtiss, S., Dixit, S., Feldt, C., et al. (2013), “Function in the human connectome: task-fMRI and individual differences in behavior,” *Neuroimage*, 80, 169–189.
- Björck, A. and Golub, G. H. (1973), “Numerical methods for computing angles between linear subspaces,” *Mathematics of Computation*, 27, 579–594.
- Buckner, R. L., Krienen, F. M., Castellanos, A., Diaz, J. C., and Thomas Yeo, B. T. (2011), “The organization of the human cerebellum estimated by intrinsic functional connectivity,” *Journal of Neurophysiology*, 106, 2322–2345.
- Campbell, J. D., Yau, C., Bowlby, R., Liu, Y., Brennan, K., Fan, H., Taylor, A. M., Wang, C., Walter, V., Akbani, R., et al. (2018), “Genomic, pathway network, and immunologic features distinguishing squamous carcinomas,” *Cell reports*, 23, 194–212.

- Carroll, J. D. (1968), “Generalization of canonical correlation analysis to three or more sets of variables,” *Proceedings of the 76th Annual Convention of the American Psychological Association*, 3, 227–228.
- Chamberlain, G. and Rothschild, M. (1983), “Arbitrage, factor structure, and mean-variance analysis on large asset markets,” *Econometrica*, 51, 1281–1304.
- Cox, D. R. (1972), “Regression models and life-tables,” *Journal of the Royal Statistical Society: Series B*, 34, 187–202.
- Crawford, K. L., Neu, S. C., and Toga, A. W. (2016), “The image and data archive at the laboratory of neuro imaging,” *Neuroimage*, 124, 1080–1083.
- Efron, B. and Tibshirani, R. J. (1993), *An Introduction to the Bootstrap*, Chapman & Hall, New York.
- Fan, J., Liao, Y., and Mincheva, M. (2013), “Large covariance estimation by thresholding principal orthogonal complements,” *Journal of the Royal Statistical Society: Series B*, 75, 603–680.
- Feng, Q., Jiang, M., Hannig, J., and Marron, J. (2018), “Angle-based joint and individual variation explained,” *Journal of Multivariate Analysis*, 166, 241–265.
- Hoadley, K. A., Yau, C., Hinoue, T., Wolf, D. M., Lazar, A. J., Drill, E., Shen, R., Taylor, A. M., Cherniack, A. D., Thorsson, V., et al. (2018), “Cell-of-origin patterns dominate the molecular classification of 10,000 tumors from 33 types of cancer,” *Cell*, 173, 291–304.
- Horn, R. A. and Johnson, C. R. (1994), *Topics in Matrix Analysis*, Cambridge University Press, Cambridge.
- Hotelling, H. (1936), “Relations between two sets of variates,” *Biometrika*, 28, 321–377.
- Huang, H. (2017), “Asymptotic behavior of support vector machine for spiked population model,” *Journal of Machine Learning Research*, 18, 1–21.
- Jensen, M. A., Ferretti, V., Grossman, R. L., and Staudt, L. M. (2017), “The NCI Genomic Data Commons as an engine for precision medicine,” *Blood*, 130, 453–459.

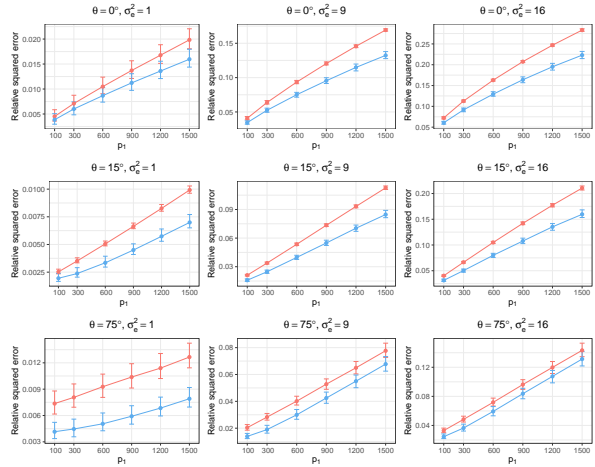
- Kettenring, J. R. (1971), "Canonical analysis of several sets of variables," *Biometrika*, 58, 433–451.
- Kishore Kumar, N. and Schneider, J. (2017), "Literature survey on low rank approximation of matrices," *Linear and Multilinear Algebra*, 65, 2212–2244.
- Koboldt, D., Fulton, R., McLellan, M., Schmidt, H., Kalicki-Veizer, J., McMichael, J., Fulton, L., Dooling, D., Ding, L., et al. (2012), "Comprehensive molecular portraits of human breast tumours," *Nature*, 490, 61–70.
- Koltchinskii, V. and Lounici, K. (2017), "Concentration inequalities and moment bounds for sample covariance operators," *Bernoulli*, 23, 110–133.
- Lam, C. and Fan, J. (2009), "Sparsistency and rates of convergence in large covariance matrix estimation," *The Annals of Statistics*, 37, 4254–4278.
- Landis, J. R. and Koch, G. G. (1977), "The measurement of observer agreement for categorical data," *Biometrics*, 33, 159–174.
- Lock, E. and Dunson, D. (2013), "Bayesian consensus clustering," *Bioinformatics*, 29, 2610–2616.
- Lock, E. F., Hoadley, K. A., Marron, J. S., and Nobel, A. B. (2013), "Joint and individual variation explained (JIVE) for integrated analysis of multiple data types," *Annals of Applied Statistics*, 7, 523–542.
- Löfstedt, T. and Trygg, J. (2011), "OnPLS—a novel multiblock method for the modelling of predictive and orthogonal variation," *Journal of Chemometrics*, 25, 441–455.
- Lu, Y., Huang, K., and Liu, C.-L. (2016), "A fast projected fixed-point algorithm for large graph matching," *Pattern Recognition*, 60, 971–982.
- Mantel, N. (1966), "Evaluation of survival data and two new rank order statistics arising in its consideration," *Cancer Chemother Rep*, 50, 163–170.

- Nadakuditi, R. R. and Silverstein, J. W. (2010), “Fundamental limit of sample generalized eigenvalue based detection of signals in noise using relatively few signal-bearing and noise-only samples,” *IEEE Journal of Selected Topics in Signal Processing*, 4, 468–480.
- O’Connell, M. J. and Lock, E. F. (2016), “R.JIVE for exploration of multi-source molecular data,” *Bioinformatics*, 32, 2877–2879.
- Olivetti, E., Sharmin, N., and Avesani, P. (2016), “Alignment of tractograms as graph matching,” *Frontiers in Neuroscience*, 10, 554.
- Onatski, A. (2010), “Determining the number of factors from empirical distribution of eigenvalues,” *The Review of Economics and Statistics*, 92, 1004–1016.
- Papadias, C. B. (2000), “Globally convergent blind source separation based on a multiuser kurtosis maximization criterion,” *IEEE Transactions on Signal Processing*, 48, 3508–3519.
- Parker, J. S., Mullins, M., Cheang, M. C., Leung, S., Voduc, D., Vickery, T., Davies, S., Fauron, C., He, X., Hu, Z., et al. (2009), “Supervised risk predictor of breast cancer based on intrinsic subtypes,” *Journal of Clinical Oncology*, 27, 1160–1167.
- Parra, L. and Sajda, P. (2003), “Blind source separation via generalized eigenvalue decomposition,” *Journal of Machine Learning Research*, 4, 1261–1269.
- Peto, R. and Peto, J. (1972), “Asymptotically efficient rank invariant test procedures,” *Journal of the Royal Statistical Society: Series A*, 135, 185–198.
- Saeed, U., Compagnone, J., Aviv, R. I., Strafella, A. P., Black, S. E., Lang, A. E., and Masellis, M. (2017), “Imaging biomarkers in Parkinson’s disease and Parkinsonian syndromes: current and emerging concepts,” *Translational Neurodegeneration*, 6, 8.
- Schouteden, M., Van Deun, K., Pattyn, S., and Van Mechelen, I. (2013), “SCA with rotation to distinguish common and distinctive information in linked data,” *Behavior Research Methods*, 45, 822–833.
- Shu, H., Wang, X., and Zhu, H. (2019), “D-CCA: A decomposition-based canonical correlation analysis for high-dimensional Datasets,” *Journal of the American Statistical Association*, doi:10.1080/01621459.2018.1543599.

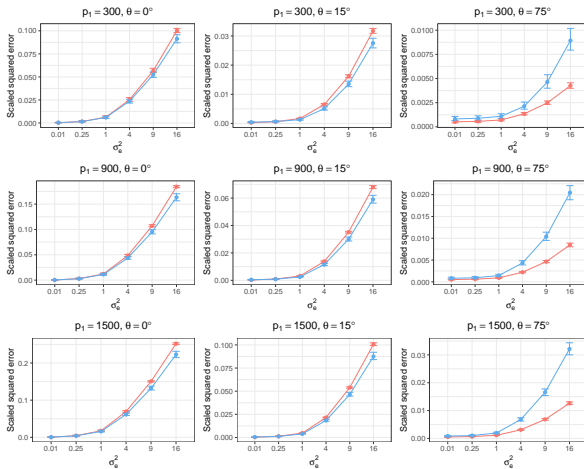
- Smilde, A. K., Westerhuis, J. A., and de Jong, S. (2003), “A framework for sequential multiblock component methods,” *Journal of Chemometrics: A Journal of the Chemometrics Society*, 17, 323–337.
- Song, Y., Schreier, P. J., Ramírez, D., and Hasija, T. (2016), “Canonical correlation analysis of high-dimensional data with very small sample support,” *Signal Processing*, 128, 449–458.
- Udell, M. and Townsend, A. (2019), “Why are big data matrices approximately low rank?” *SIAM Journal on Mathematics of Data Science*, 1, 144–160.
- Van Essen, D. C., Smith, S. M., Barch, D. M., Behrens, T. E., Yacoub, E., Ugurbil, K., Consortium, W.-M. H., et al. (2013), “The WU-Minn human connectome project: an overview,” *Neuroimage*, 80, 62–79.
- Wang, W. and Fan, J. (2017), “Asymptotics of empirical eigenstructure for high dimensional spiked covariance,” *The Annals of Statistics*, 45, 1342–1374.
- Ward, Jr., J. H. (1963), “Hierarchical grouping to optimize an objective function,” *Journal of the American Statistical Association*, 58, 236–244.
- Weiner, M. W., Veitch, D. P., Aisen, P. S., Beckett, L. A., Cairns, N. J., Green, R. C., Harvey, D., Jack, C. R., Jagust, W., Liu, E., et al. (2013), “The Alzheimer’s Disease Neuroimaging Initiative: a review of papers published since its inception,” *Alzheimer’s & Dementia*, 9, e111–e194.
- Yin, Y.-Q., Bai, Z.-D., and Krishnaiah, P. R. (1988), “On the limit of the largest eigenvalue of the large dimensional sample covariance matrix,” *Probability Theory and Related Fields*, 78, 509–521.
- Yu, Y., Wang, T., and Samworth, R. J. (2015), “A useful variant of the Davis–Kahan theorem for statisticians,” *Biometrika*, 102, 315–323.
- Zhou, G., Cichocki, A., Zhang, Y., and Mandic, D. P. (2016), “Group component analysis for multiblock data: Common and individual feature extraction,” *IEEE Transactions on Neural Networks and Learning Systems*, 27, 2426–2439.



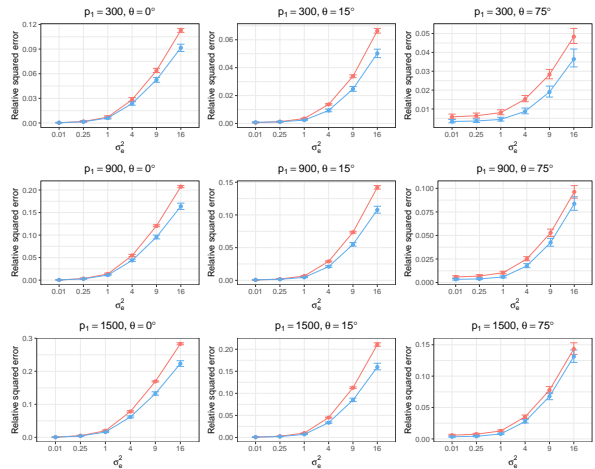
(a) Scaled squared error with varying p_1



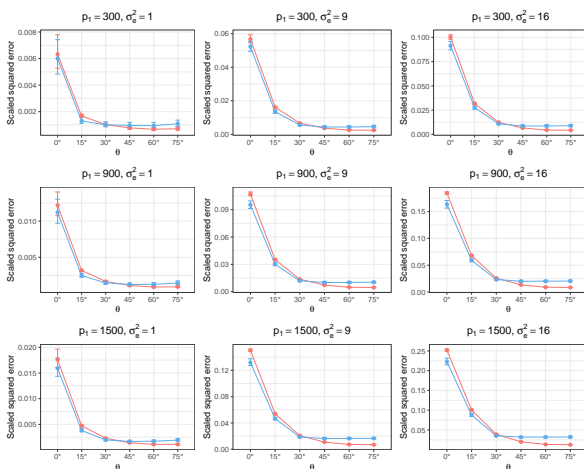
(b) Relative squared error with varying p_1



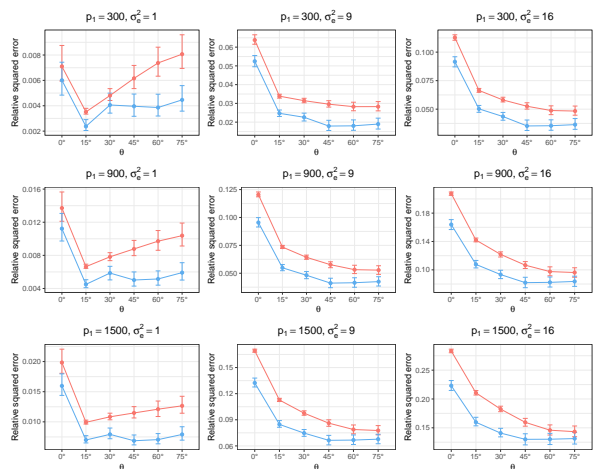
(c) Scaled squared error with varying σ_e^2



(d) Relative squared error with varying σ_e^2

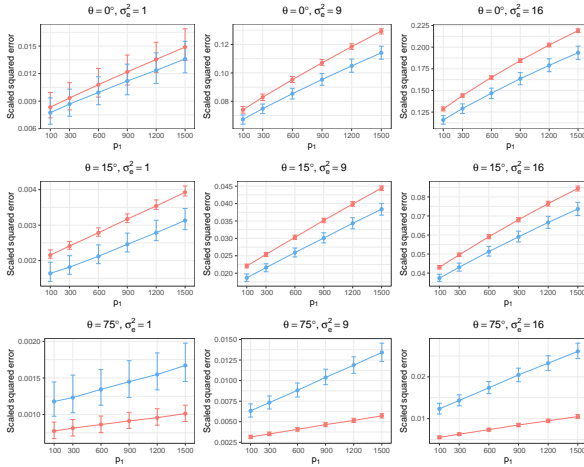


(e) Scaled squared error with varying θ

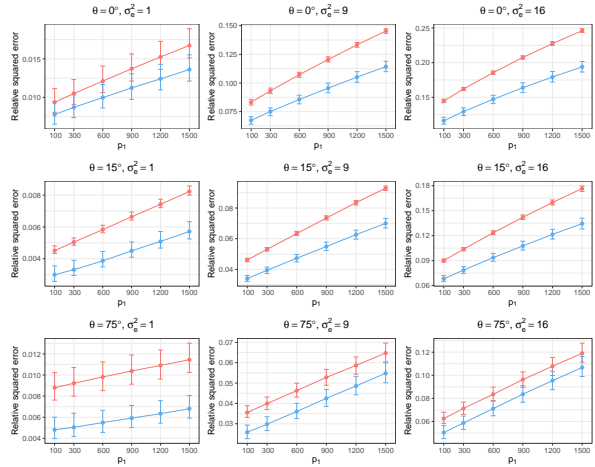


(f) Relative squared error with varying θ

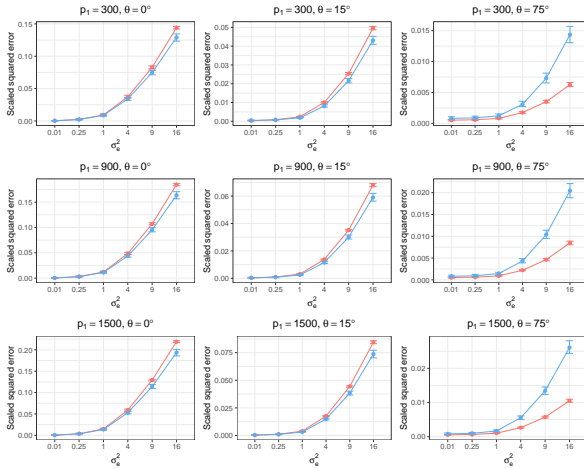
Figure S.1. Simulation results for Setup 1: medians and interquartile ranges of the scaled squared error $2\|\widehat{\mathbf{C}} - \mathbf{C}\|_{\star}^2 / (\|\mathbf{X}_1^S\|_{\star}^2 + \|\mathbf{X}_2^S\|_{\star}^2)$ and the relative squared error $\|\widehat{\mathbf{C}} - \mathbf{C}\|_{\star}^2 / \|\mathbf{C}\|_{\star}^2$ over 1000 replications in the Frobenius norm (red) and the spectral norm (blue).



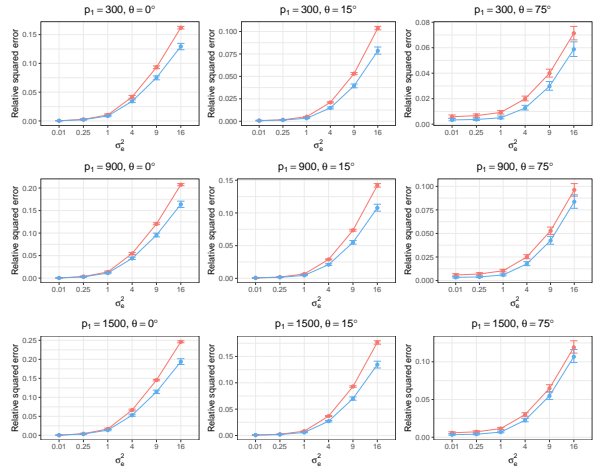
(a) Scaled squared error with varying p_1



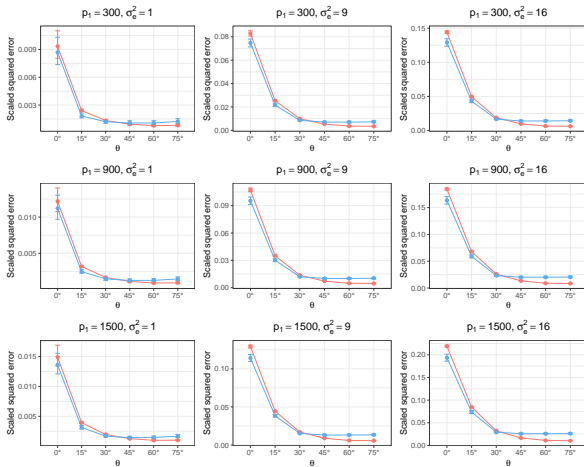
(b) Relative squared error with varying p_1



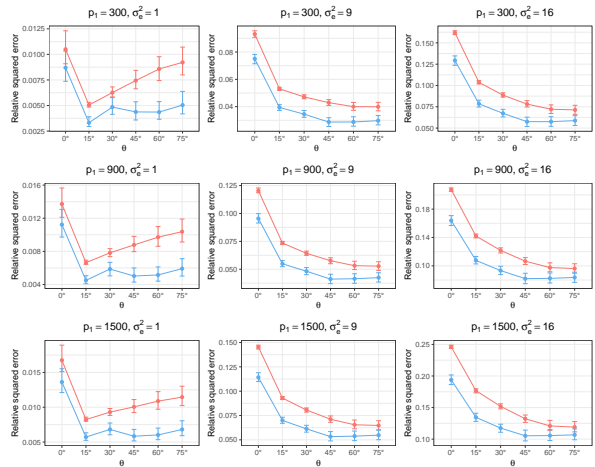
(c) Scaled squared error with varying σ_e^2



(d) Relative squared error with varying σ_e^2



(e) Scaled squared error with varying θ



(f) Relative squared error with varying θ

Figure S.2. Simulation results for Setup 2: medians and interquartile ranges of the scaled squared error $2\|\hat{C} - C\|_*^2 / (\|\mathbf{X}_1^S\|_*^2 + \|\mathbf{X}_2^S\|_*^2)$ and the relative squared error $\|\hat{C} - C\|_*^2 / \|C\|_*^2$ over 1000 replications in the Frobenius norm (red) and the spectral norm (blue).

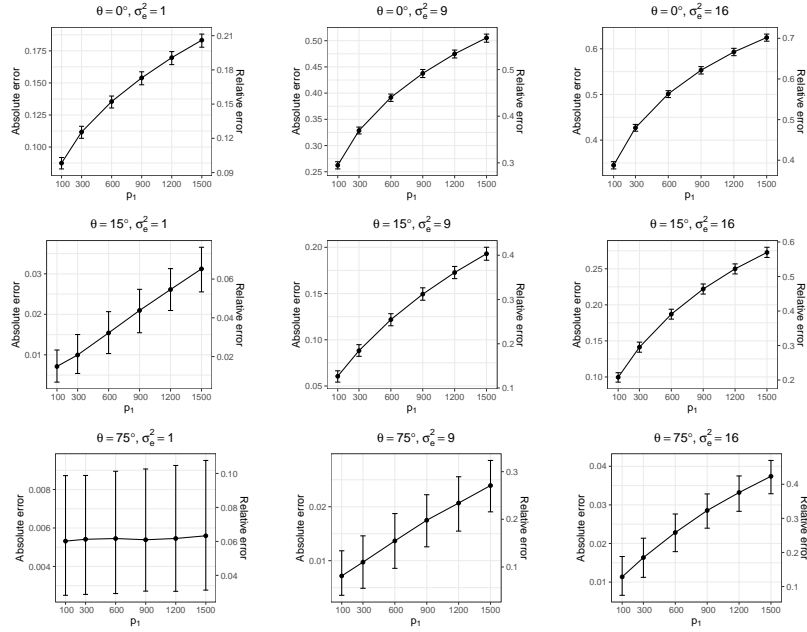


Figure S.3. Simulation results for Setup 1: medians and interquartile ranges of the absolute error $|\text{tr}(\frac{1}{n}\widehat{\mathbf{C}}\widehat{\mathbf{C}}^\top) - \text{tr}\{\text{cov}(\mathbf{c})\}|$ and the relative error $|\text{tr}(\frac{1}{n}\widehat{\mathbf{C}}\widehat{\mathbf{C}}^\top)/\text{tr}\{\text{cov}(\mathbf{c})\} - 1|$ over 1000 replications with varying p_1 .

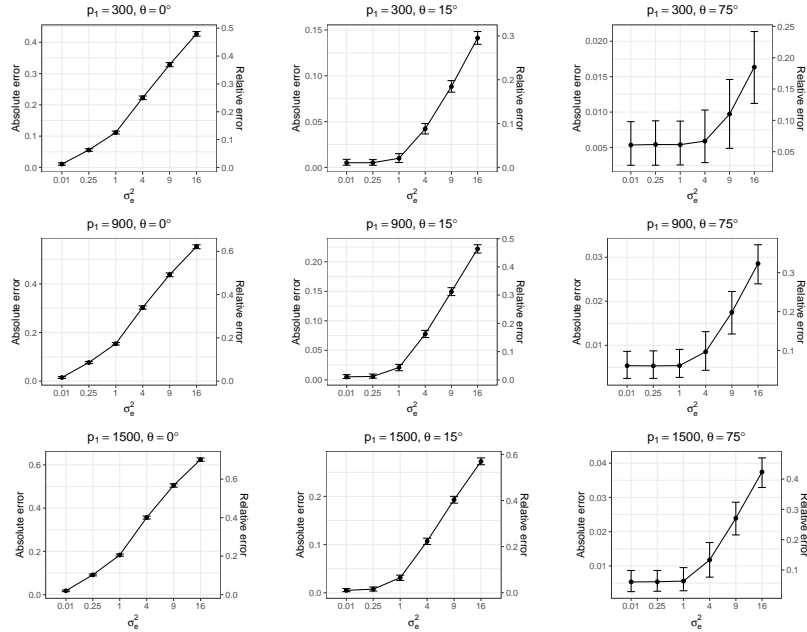


Figure S.4. Simulation results for Setup 1: medians and interquartile ranges of the absolute error $|\text{tr}(\frac{1}{n}\widehat{\mathbf{C}}\widehat{\mathbf{C}}^\top) - \text{tr}\{\text{cov}(\mathbf{c})\}|$ and the relative error $|\text{tr}(\frac{1}{n}\widehat{\mathbf{C}}\widehat{\mathbf{C}}^\top)/\text{tr}\{\text{cov}(\mathbf{c})\} - 1|$ over 1000 replications with varying σ_e^2 .

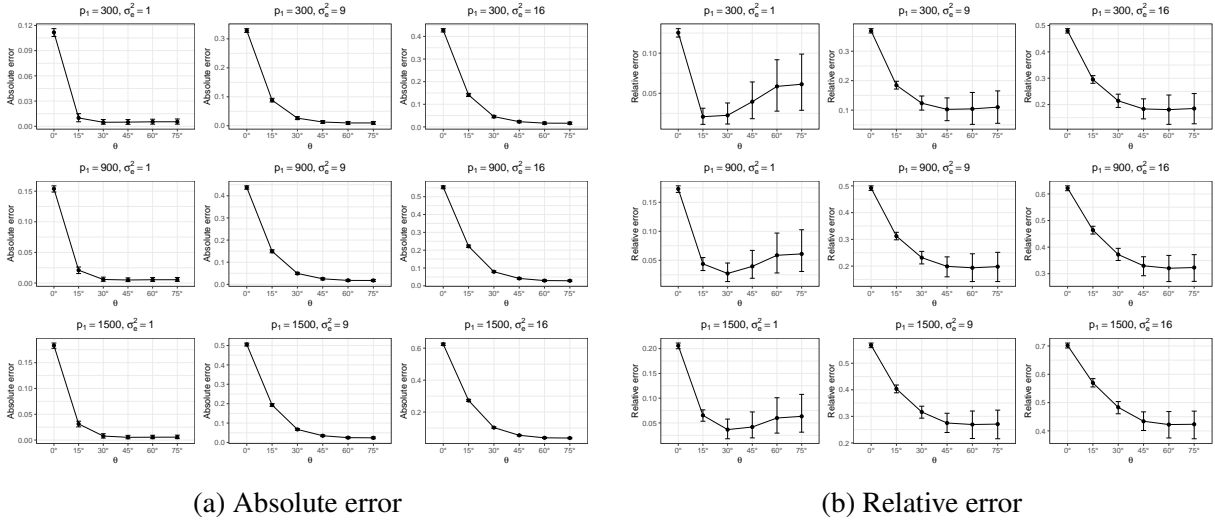


Figure S.5. Simulation results for Setup 1: medians and interquartile ranges of the absolute error $|\text{tr}(\frac{1}{n}\widehat{\mathbf{C}}\widehat{\mathbf{C}}^\top) - \text{tr}\{\text{cov}(\mathbf{c})\}|$ and the relative error $|\text{tr}(\frac{1}{n}\widehat{\mathbf{C}}\widehat{\mathbf{C}}^\top)/\text{tr}\{\text{cov}(\mathbf{c})\} - 1|$ over 1000 replications with varying θ .

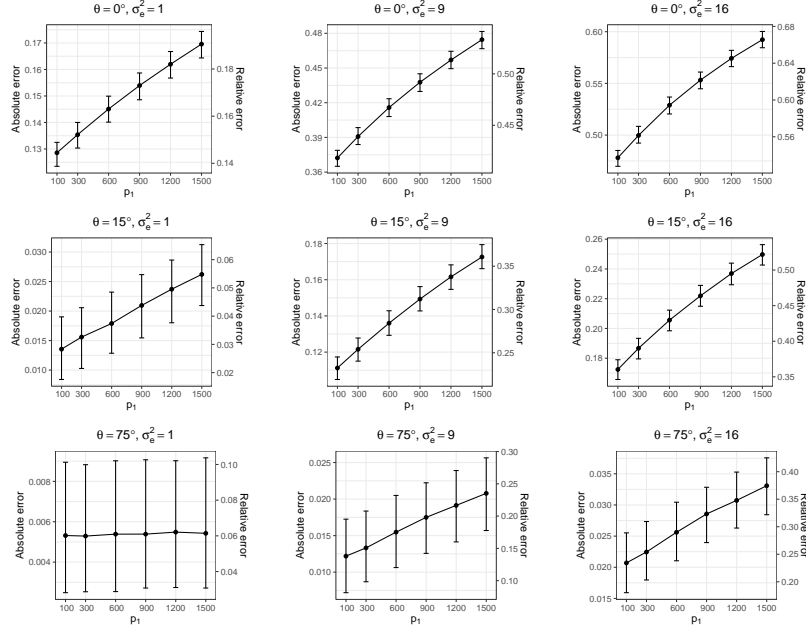


Figure S.6. Simulation results for Setup 2: medians and interquartile ranges of the absolute error $|\text{tr}(\frac{1}{n}\widehat{\mathbf{C}}\widehat{\mathbf{C}}^\top) - \text{tr}\{\text{cov}(\mathbf{c})\}|$ and the relative error $|\text{tr}(\frac{1}{n}\widehat{\mathbf{C}}\widehat{\mathbf{C}}^\top)/\text{tr}\{\text{cov}(\mathbf{c})\} - 1|$ over 1000 replications with varying p_1 .

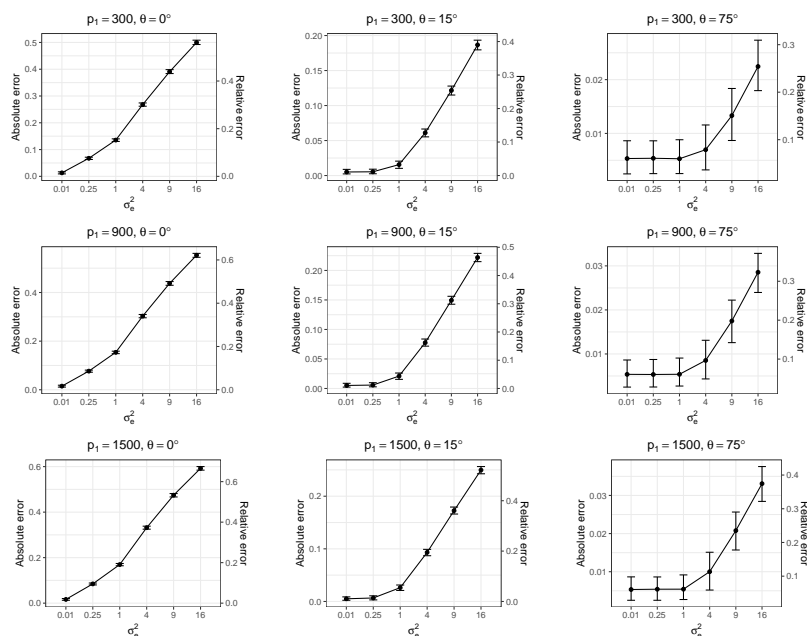


Figure S.7. Simulation results for Setup 2: medians and interquartile ranges of the absolute error $|\text{tr}(\frac{1}{n}\widehat{\mathbf{C}}\widehat{\mathbf{C}}^\top) - \text{tr}\{\text{cov}(\mathbf{e})\}|$ and the relative error $|\text{tr}(\frac{1}{n}\widehat{\mathbf{C}}\widehat{\mathbf{C}}^\top)/\text{tr}\{\text{cov}(\mathbf{e})\} - 1|$ over 1000 replications with varying σ_e^2 .

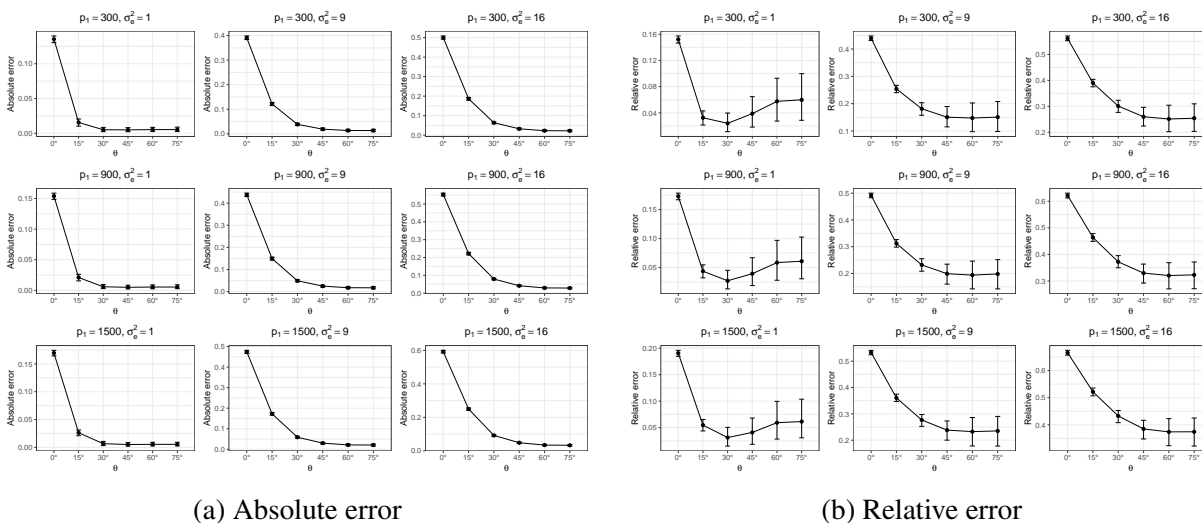


Figure S.8. Simulation results for Setup 2: medians and interquartile ranges of the absolute error $|\text{tr}(\frac{1}{n}\widehat{\mathbf{C}}\widehat{\mathbf{C}}^\top) - \text{tr}\{\text{cov}(\mathbf{e})\}|$ and the relative error $|\text{tr}(\frac{1}{n}\widehat{\mathbf{C}}\widehat{\mathbf{C}}^\top)/\text{tr}\{\text{cov}(\mathbf{e})\} - 1|$ over 1000 replications with varying θ .

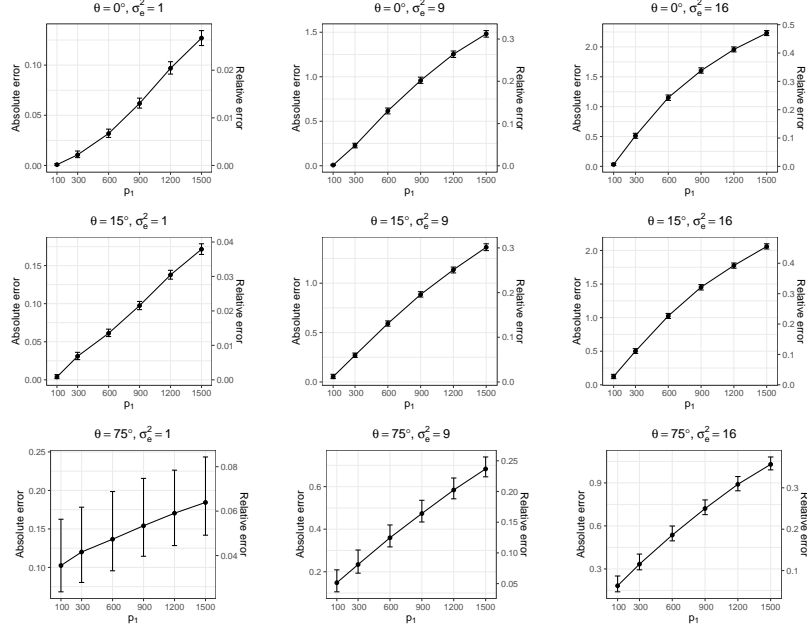


Figure S.9. Simulation results for Setup 1: medians and interquartile ranges of the absolute error $|\text{tr}(\mathbf{Q}_1^\top \hat{\mathbf{P}}_a \mathbf{Q}_{2A} (\mathbf{Q}_1^\top \hat{\mathbf{P}}_a \mathbf{Q}_{2A})^\top) - \text{tr}(\mathbf{Q}_1^\top \mathbf{P}_a \mathbf{Q}_{2A} (\mathbf{Q}_1^\top \mathbf{P}_a \mathbf{Q}_{2A})^\top)|$ and the relative error $|\text{tr}(\mathbf{Q}_1^\top \hat{\mathbf{P}}_a \mathbf{Q}_{2A} (\mathbf{Q}_1^\top \hat{\mathbf{P}}_a \mathbf{Q}_{2A})^\top) / \text{tr}(\mathbf{Q}_1^\top \mathbf{P}_a \mathbf{Q}_{2A} (\mathbf{Q}_1^\top \mathbf{P}_a \mathbf{Q}_{2A})^\top) - 1|$ over 1000 replications with varying p_1 .

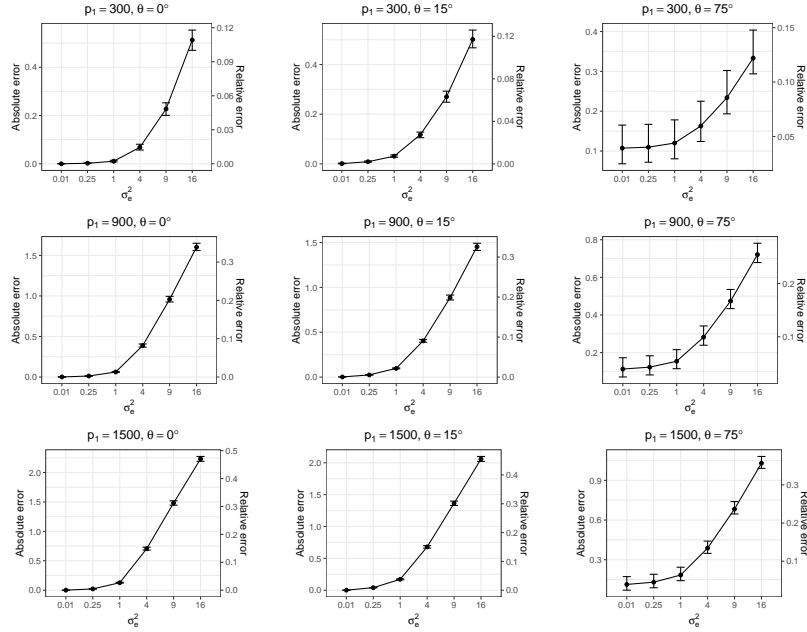


Figure S.10. Simulation results for Setup 1: medians and interquartile ranges of the absolute error $|\text{tr}(\mathbf{Q}_1^\top \hat{\mathbf{P}}_a \mathbf{Q}_{2A} (\mathbf{Q}_1^\top \hat{\mathbf{P}}_a \mathbf{Q}_{2A})^\top) - \text{tr}(\mathbf{Q}_1^\top \mathbf{P}_a \mathbf{Q}_{2A} (\mathbf{Q}_1^\top \mathbf{P}_a \mathbf{Q}_{2A})^\top)|$ and the relative error $|\text{tr}(\mathbf{Q}_1^\top \hat{\mathbf{P}}_a \mathbf{Q}_{2A} (\mathbf{Q}_1^\top \hat{\mathbf{P}}_a \mathbf{Q}_{2A})^\top) / \text{tr}(\mathbf{Q}_1^\top \mathbf{P}_a \mathbf{Q}_{2A} (\mathbf{Q}_1^\top \mathbf{P}_a \mathbf{Q}_{2A})^\top) - 1|$ over 1000 replications with varying σ_e^2 .

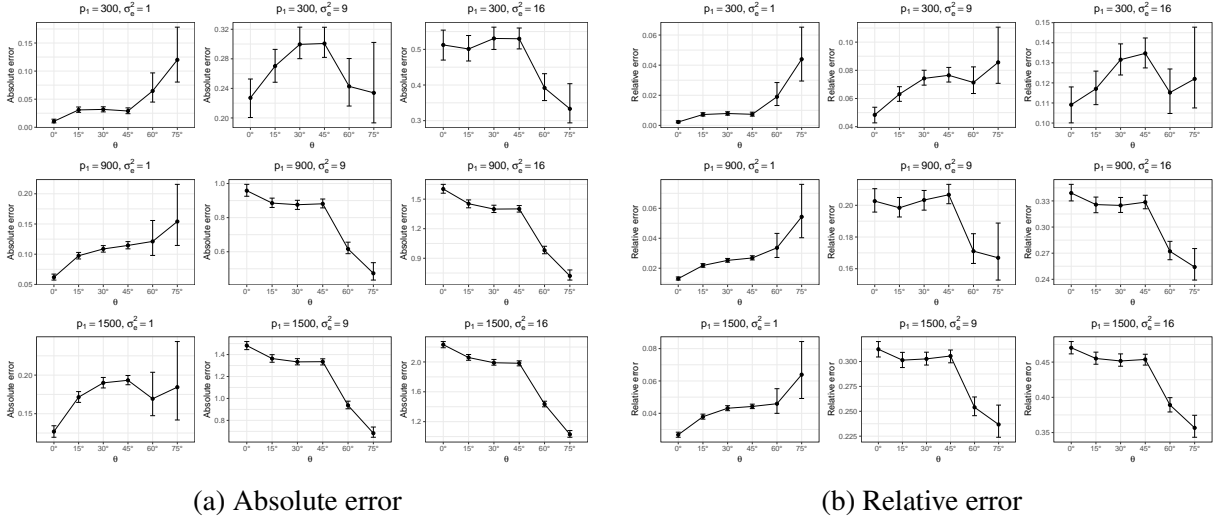


Figure S.11. Simulation results for Setup 1: medians and interquartile ranges of the absolute error $|\text{tr}(\mathbf{Q}_1^\top \hat{\mathbf{P}}_a \mathbf{Q}_{2A} (\mathbf{Q}_1^\top \hat{\mathbf{P}}_a \mathbf{Q}_{2A})^\top) - \text{tr}(\mathbf{Q}_1^\top \mathbf{P}_a \mathbf{Q}_{2A} (\mathbf{Q}_1^\top \mathbf{P}_a \mathbf{Q}_{2A})^\top)|$ and the relative error $|\text{tr}(\mathbf{Q}_1^\top \hat{\mathbf{P}}_a \mathbf{Q}_{2A} (\mathbf{Q}_1^\top \hat{\mathbf{P}}_a \mathbf{Q}_{2A})^\top) / \text{tr}(\mathbf{Q}_1^\top \mathbf{P}_a \mathbf{Q}_{2A} (\mathbf{Q}_1^\top \mathbf{P}_a \mathbf{Q}_{2A})^\top) - 1|$ over 1000 replications with varying θ .

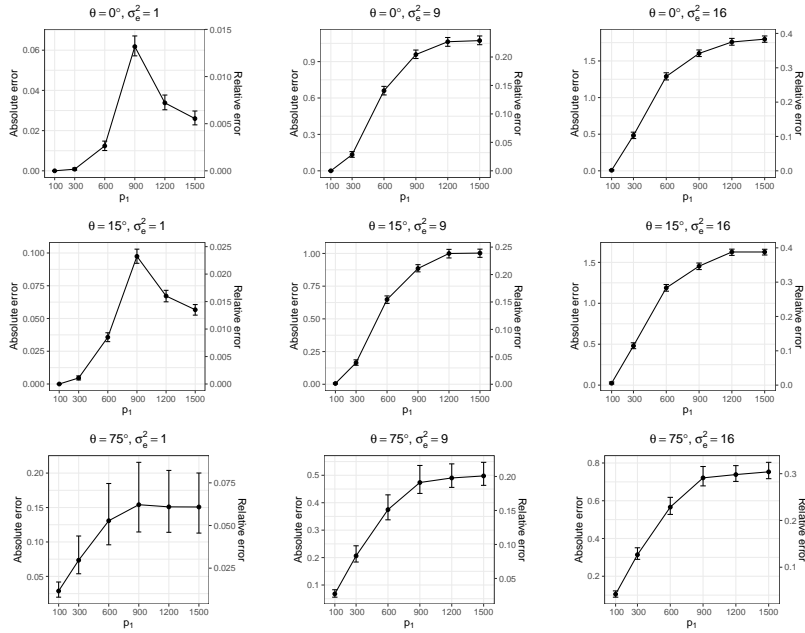


Figure S.12. Simulation results for Setup 2: medians and interquartile ranges of the absolute error $|\text{tr}(\mathbf{Q}_1^\top \hat{\mathbf{P}}_a \mathbf{Q}_{2A} (\mathbf{Q}_1^\top \hat{\mathbf{P}}_a \mathbf{Q}_{2A})^\top) - \text{tr}(\mathbf{Q}_1^\top \mathbf{P}_a \mathbf{Q}_{2A} (\mathbf{Q}_1^\top \mathbf{P}_a \mathbf{Q}_{2A})^\top)|$ and the relative error $|\text{tr}(\mathbf{Q}_1^\top \hat{\mathbf{P}}_a \mathbf{Q}_{2A} (\mathbf{Q}_1^\top \hat{\mathbf{P}}_a \mathbf{Q}_{2A})^\top) / \text{tr}(\mathbf{Q}_1^\top \mathbf{P}_a \mathbf{Q}_{2A} (\mathbf{Q}_1^\top \mathbf{P}_a \mathbf{Q}_{2A})^\top) - 1|$ over 1000 replications with varying p_1 .

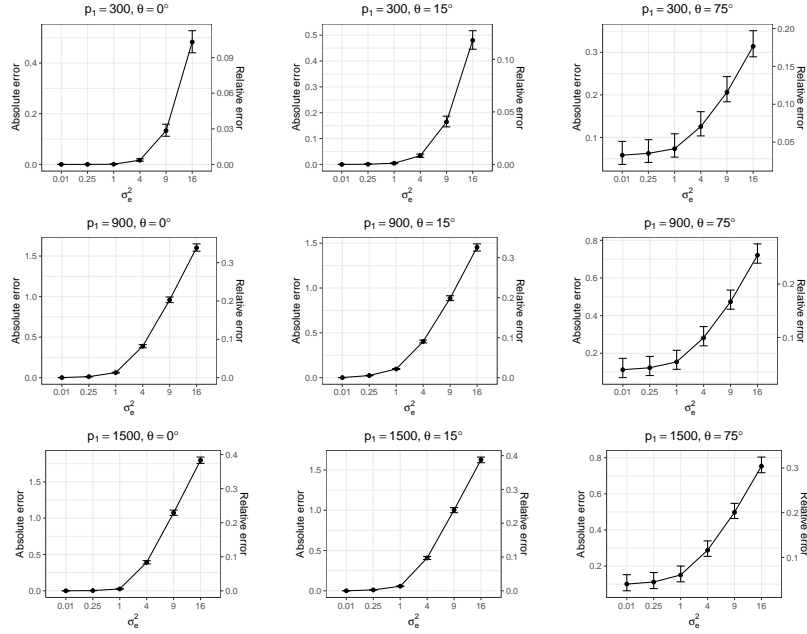
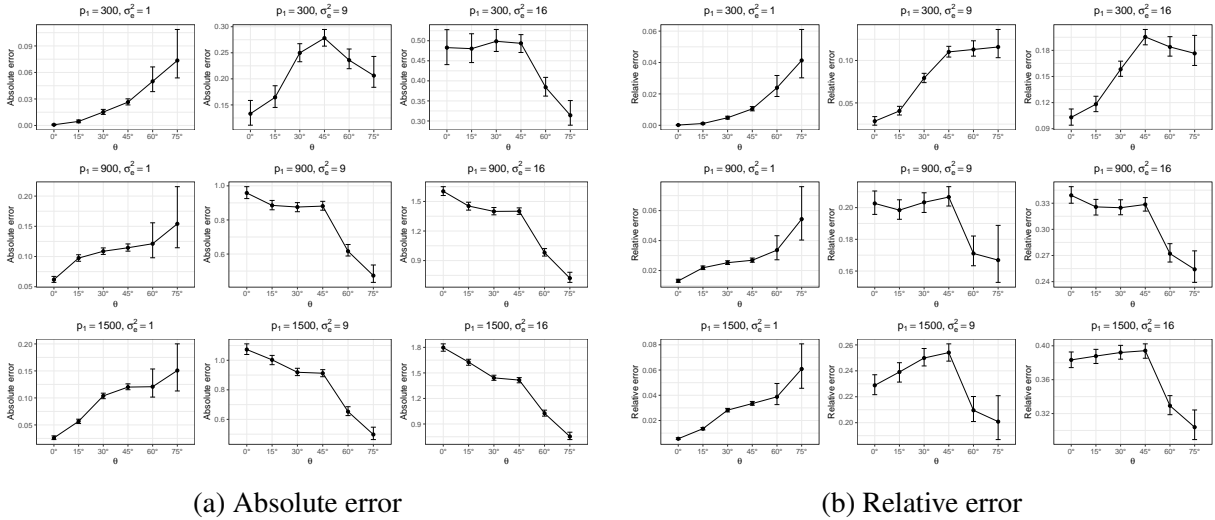


Figure S.13. Simulation results for Setup 2: medians and interquartile ranges of the absolute error $|\text{tr}(\mathbf{Q}_1^\top \hat{\mathbf{P}}_a \mathbf{Q}_{2A} (\mathbf{Q}_1^\top \hat{\mathbf{P}}_a \mathbf{Q}_{2A})^\top) - \text{tr}(\mathbf{Q}_1^\top \mathbf{P}_a \mathbf{Q}_{2A} (\mathbf{Q}_1^\top \mathbf{P}_a \mathbf{Q}_{2A})^\top)|$ and the relative error $|\text{tr}(\mathbf{Q}_1^\top \hat{\mathbf{P}}_a \mathbf{Q}_{2A} (\mathbf{Q}_1^\top \hat{\mathbf{P}}_a \mathbf{Q}_{2A})^\top) / \text{tr}(\mathbf{Q}_1^\top \mathbf{P}_a \mathbf{Q}_{2A} (\mathbf{Q}_1^\top \mathbf{P}_a \mathbf{Q}_{2A})^\top) - 1|$ over 1000 replications with varying σ_e^2 .



(a) Absolute error

(b) Relative error

Figure S.14. Simulation results for Setup 2: medians and interquartile ranges of the absolute error $|\text{tr}(\mathbf{Q}_1^\top \hat{\mathbf{P}}_a \mathbf{Q}_{2A} (\mathbf{Q}_1^\top \hat{\mathbf{P}}_a \mathbf{Q}_{2A})^\top) - \text{tr}(\mathbf{Q}_1^\top \mathbf{P}_a \mathbf{Q}_{2A} (\mathbf{Q}_1^\top \mathbf{P}_a \mathbf{Q}_{2A})^\top)|$ and the relative error $|\text{tr}(\mathbf{Q}_1^\top \hat{\mathbf{P}}_a \mathbf{Q}_{2A} (\mathbf{Q}_1^\top \hat{\mathbf{P}}_a \mathbf{Q}_{2A})^\top) / \text{tr}(\mathbf{Q}_1^\top \mathbf{P}_a \mathbf{Q}_{2A} (\mathbf{Q}_1^\top \mathbf{P}_a \mathbf{Q}_{2A})^\top) - 1|$ over 1000 replications with varying θ .